Exosomes Released from Senescent Cells and Circulatory Exosomes Isolated from Human Plasma Reveal Aging-associated Proteomic and Lipid Signatures

Sandip Kumar Patel[1#], Joanna Bons[1#], Jacob P. Rose[1], Jessie R. Chappel[2], Rebecca L. Beres[3], Mark A. Watson[1], Corey Webster[1], Jordan B. Burton[1], Roland Bruderer[4], Pierre-Yves Desprez[1,5], Lukas Reiter[4], Judith Campisi[1], Erin S. Baker[3], and Birgit Schilling[1,*]

[1]The Buck Institute for Research on Aging, Novato, CA 94945, USA

[2]Bioinformatics Research Center, Department of Biological Sciences, North Carolina State University, Raleigh, NC 27606, USA

[3]Department of Chemistry, University of North Carolina at Chapel Hill, NC 27514, USA

[4]Biognosys AG, 8952 Schlieren, Switzerland

[5]California Pacific Medical Centre, Research Institute, San Francisco, CA 94107, USA

[#] These authors contributed equally (co-first authors)

* Correspondence: Birgit Schilling, Buck Institute for Research on Aging, 8001 Redwood Blvd, Novato, CA 94945, USA; Email: bschilling@buckinstitute.org

Abstract

Senescence emerged as significant mechanism of aging and age-related diseases, offering an attractive target for clinical interventions. Senescent cells release a senescence-associated secretory phenotype (SASP), including exosomes that may act as signal transducers between distal tissues, propagating secondary or bystander senescence and signaling throughout the body. However, the composition of exosome SASP remains underexplored, presenting an opportunity for novel unbiased discovery. We present a detailed proteomic and lipidomic analysis of exosome SASP using mass spectrometry from human plasma from young and older individuals and from tissue culture of senescent primary human lung fibroblasts. We identified ~1,300 exosome proteins released by senescent cells induced by three different senescence inducers. In parallel, a human plasma cohort from young (20–26 years) and old (65–74 years) individuals revealed over 1,350 exosome proteins and 171 plasma exosome proteins were regulated when comparing old vs young individuals. Of the age-regulated plasma exosome proteins, we observed 52 exosome SASP factors that were also regulated in exosomes from the senescent fibroblasts, including serine protease inhibitors (SERPINs), Prothrombin, Coagulation factor V, Plasminogen, and Reelin. 247 lipids were identified in exosome samples. Following senescence induction, identified phosphatidylcholines, phosphatidylethanolamines, and sphingomyelins increased significantly indicating cellular membrane changes. Interestingly, significantly changed proteins were related to extracellular matrix remodeling and inflammation, both potentially detrimental pathways that can damage surrounding tissues and even induce secondary senescence. Our findings reveal mechanistic insights and potential senescence biomarkers, enabling a better approach to surveilling the senescence burden in the aging population and offering therapeutic targets for interventions.

Keywords (5 words): Proteomics, senescence, exosome senescence-associated secretory phenotype (SASP), data-independent acquisitions, aging

Introduction

The World Health Organization (WHO) estimates that one out of every six individuals in the world will be aged 60 or older by 2030 [1]. This demographic shift will have far-reaching social, economic, and healthcare implications. The aging population is at an increased risk for chronic diseases, which could result in a significant public health crisis [2, 3]. Therefore, there is a critical need to prioritize healthy aging, which begins with comprehending the fundamental molecular basis of aging to identify potential interventions and biomarkers.

Cellular senescence is considered a crucial mechanism of aging because senescent cells accumulate in different tissues over time and contribute to the aging process [4]. Senescence is the process by which cells become cell cycle arrested while still staying viable, metabolically active, and undergoing distinct phenotypic alterations. Senescence can be induced by various intrinsic factors, such as telomer shortening (Hayflick's limit) [5], by extrinsic factors, such as irradiation (IR) and chemical reagents (e.g., doxorubicin, doxo), or via Mitochondrial Dysfunction-Associated Senescence (MiDAS) [6, 7]. The various senescence inducers all exhibit varied modes of action, for example, irradiation causes double-stranded breaks in DNA [8], doxorubicin induces DNA cross-linking [9], while disruption in normal mitochondrial function results in MiDAS [6]. Senescent cells exert their pleiotropic biological effects by secretion of senescence-associated secretory phenotype (SASP) [10-12]. The SASP represents a myriad of pro-inflammatory molecules, growth factors, extracellular matrix (ECM) metalloproteinases, microRNAs, and lipids that are either directly secreted or packaged into exosomes [13-15].

Exosomes are small, lipid-bilayer enclosed nanoparticles derived from cells with a diameter ranging between 30 nm and 150 nm. They are known to transport various biomolecules to recipient cells in a paracrine or endocrine manner, allowing them to act as signal transducers between distal tissues [16]. The cargo carried by circulating exosomes includes proteins, lipids, miRNA and other components, which all have been implicated in aging and age-related diseases [17]. However, the comprehensive characterization of exosome SASP and their role in potentially propagating senescence (secondary/bystander senescence) and how they may influence the aging progression is still largely understudied. Several challenges include sub-optimal enrichment strategies that are compatible with mass spectrometry technologies and protein contamination from biofluids, which often impede downstream omics processing [18].

Current methods for isolating exosomes commonly rely on physical properties of extracellular vesicles (EVs) or target-specific surface markers [19]. A novel approach, Mag-Net, enriches extracellular vesicles from plasma through electrostatic interactions, providing a promising alternative [20]. Ultracentrifugation is one of the more common methods for exosome enrichment [21]. However, this low-throughput method can lead to contamination from other EVs, high molecular weight proteins, and highly abundant proteins. To enhance exosome purity, size exclusion chromatography (SEC) is often used before centrifugation or filtration [22]. Developing high-throughput workflows for identifying and quantifying circulating exosome SASP components (secreted from various senescent cell types) in plasma is a valuable resource for characterizing cellular senescence signatures by identifying (i) specific affected tissues, (ii) biomarkers to measure biological age non-invasively, and (iii) novel targets for anti-aging therapeutics.

In this study, we developed a platform to enrich exosomes from plasma and tissue culture for the analysis of exosomal proteins, lipids, and miRNA (Fig. 1). Additionally, we generated a novel “human exosome protein spectral library” using data-dependent acquisition (DDA) and performed data-independent acquisition (DIA) workflows for exosome protein quantification. This development introduces quantitative plasma exosome workflows, where DIA-MS acquisitions [23, 24] are searched efficiently in Spectronaut (Biognosys). Our study showed that senescent fibroblasts induced by three stimuli (IR, doxo, and Antimycin A-induced MiDAS) released highly complex and dynamic overlapping exosome profiles, some of which overlap with profiles we also observed in the human plasma exosomes from older individuals. Importantly, in exosomes from senescent cells we identified many categories of significantly changing proteins related to extracellular matrix remodeling and inflammation, which are both implicated in accelerating secondary senescence. Our study aims to address several critical knowledge gaps in the field of exosome-associated SASP, including identifying aging-specific exosome signatures, cell-specific contributions, and local versus systemic effects. We also explore molecular pathways through which exosomes propagate senescence, inflammation, and tissue remodeling. To advance this understanding, we optimized exosome isolation workflows from both cell culture and plasma, enabling robust multi-omics analyses. Our study has identified and quantified exosome cargo, including not only proteins but also significantly altered lipids and miRNAs. These findings enhance our understanding of exosome composition in aging and

106 provide a foundation for developing senescence-targeted diagnostics and therapeutics to
107 manage age-associated diseases and promote healthy aging.
108
109 **Results**
110 **Exosome enrichment workflow from a plasma aging cohort and from primary cultured**
111 **senescent cells.**
112 We performed a comprehensive proteomic analysis of exosome SASP from senescent primary
113 human lung fibroblast cells (IMR90) induced by three different stimuli, irradiation (IR),
114 doxorubicin (doxo), and Antimycin A-induced MiDAS. Furthermore, we profiled the proteome
115 and miRNA contained in exosomes from plasma from young (20-26 years old) and older (65-74
116 years old) individuals (Fig.1).
117
118 To improve the purity of exosome enrichment for downstream processing we developed
119 a robust workflow for exosome enrichment using sequential size-exclusion chromatography
120 (SEC) followed by ultrafiltration (SEC/UF) or SEC followed by ultracentrifugation (SEC/UC; Fig.
121 S1a). Both SEC/UC and SEC/UF yielded equivalent protein groups identification for exosomes
122 by mass spectrometric proteomics analysis (Fig. S1b). With consideration for ease, time, and
123 cost-effectiveness, we proceeded with SEC/UF for downstream proteomics and miRNA analysis
124 (Fig. 2A). The details of SEC elution and pooling strategies are provided in Fig. 2B. Twenty SEC-
125 extracted plasma fractions (1 mL each) were initially analyzed by spectrophotometry as a crude
126 assessment of exosome enrichment (15-35 mL in the fractionation scheme). The majority of
127 plasma exosomes were eluted within the first 10 fractions (*i.e.* 10 mL), whereas contaminating
128 plasma proteins eluted more slowly, with a maximum protein concentration achieved by the
129 20th fraction (Fig. 2C). A pool of all the fractions containing exosomes were estimated to have
130 $\sim 1\times10^{10}$ exosome particles per mL of plasma with a qNano Gold nanoparticle characterization
131 instrument, which uses tunable resistive pulse sensing to measure particles (Fig. 2D). For
132 immunoblotting, from the 10 mL containing exosomes (Fig. 2C) we pooled each two consecutive
133 fractions into one, resulting in a total of five exosome-enriched fractions (E1–E5), one post-EV
134 fraction (P1), and a pooled soluble protein fraction (P10) containing all subsequent fractions (Fig.
135 2B). Fractions E2–E5 stained positively for the exosome-specific protein markers CD9 (27 kDa)
136 and Tumour Susceptibility Gene 101 (TSG101; 44 kDa; Fig. 2E-F). Using the SEC/UF workflow,

137 we observed more intense bands for exosome-specific markers and less contaminating bands
138 from protein contaminants IgG and albumin (which pose challenges in downstream proteomic
139 analysis) compared to UC (Fig. 2E-F). These results highlighted our rational to proceed with the
140 SEC/UF approach. Correspondingly, we also performed exosome enrichment and subsequent
141 exosome quality control (QC) for exosomes from human primary fibroblasts IMR90 (Fig. S1c).
142 Overall, our SEC/UF workflow led to highly enriched, intact, and 'contaminant-free' (certainly
143 contaminant- reduced) exosomes from both isolation schemes either from human plasma as
144 well as from human primary fibroblasts. The biological outcomes and pathways are discussed
145 in the below sections.
146

147 **Mass spectrometric quantification of exosome protein cargo via label-free data-**
148 **independent acquisition (DIA).**

149 Data-independent acquisition (DIA)-mass spectrometry (MS) provides comprehensive and
150 highly quantitative workflows for protein identification analyzing complex biological matrices,
151 such as plasma, but also from more specialized 'sub-compartments', such as exosomes and/or
152 extracellular vehicles. DIA-MS [23-25] approaches have tremendously enhanced protein
153 coverage, deep protein profiling and quantitative precision by employing an unbiased MS/MS
154 data acquisition of precursor ions, leading to confident and reproducible peptide identification
155 and quantification across biological replicates. To optimally search using mass spectrometric
156 spectral libraries for data processing, we developed custom, in-house spectral libraries for
157 human plasma-exosome samples from five young (20–26 years) and five older (65-74 years)
158 individuals (Table S1), using two different data acquisition approaches (Fig. 1). The first
159 approach using data-dependent acquisition (DDA) built a comprehensive exosome spectral
160 library from highly fractionated samples, that served as a resource for future work, and that can
161 be applied to any future DIA-MS analyses of human exosome samples. More specifically, we
162 generated a DDA spectral library from DDA acquisitions of 25 generated reversed-phase
163 fractions from pooled plasma exosome proteins. A total of 2,323 protein groups was identified
164 upon processing with the Spectronaut (Biognosys) search algorithm (Fig. S2A; Table S2A),
165 among which 1,902 protein groups were identified with at least two unique peptides (Table S2B).
166 The second approach using data-independent acquisition (DIA) was introduced to feature a
167 robust, precise, and straightforward methodology that does not require an up-front generation of

168 deep spectral libraries by fractionation, which can be time-consuming, labor-intensive, and
169 typically requires a larger amount of starting material. Plasma exosome samples from 10 human
170 individuals were subjected to DIA-MS analysis and subsequently processed using the directDIA
171 algorithm within Spectronaut. We also combined the DDA and directDIA spectral libraries to
172 develop a hybrid library consisting of overall 2,225 protein groups (Fig. S2A; Table S2E), of
173 which 1,808 proteins were identified with at least two unique peptides (Table S2F). The hybrid
174 spectral library was used to search the plasma exosome DIA-MS data reported in this study
175 (Table S2F). For more details regarding the spectral library approaches and additional metrics
176 and quality control, as well as comparisons with other publicly available biofluid exosome
177 datasets (urine exosomes [26]), please see Figure S2 and Table S2A-H. Our generated hybrid
178 spectral library showed an overlap of 79% with the Plasma Exocarta database [27], confirming
179 a highly enriched and robust isolated exosome proteins. Interestingly, 370 (~21%) plasma
180 exosome proteins were uniquely identified in our study (Fig. S2H), potentially representing novel
181 plasma exosome proteins.

182 **Distinct exosome SASP protein profiles obtained from senescent human primary lung**
183 **fibroblasts exposed to different senescence inducers.**

184 To evaluate the impact of different senescence stimuli on exosome SASP proteins, we induced
185 senescence in human primary fibroblasts by (a) Irradiation (IR), (b) doxorubicin (doxo), and (c)
186 Antimycin A (MiDAS) (Fig. 3A (i)). Either quiescent (Qui) or DMSO-treated (DMSO) fibroblasts
187 were used as a control. Each senescence stimulus and the control group comprised four
188 biological replicates. Fig. 3A (ii) provides a detailed account of the exosome SASP collection
189 following senescence induction. Briefly, we induced senescence in fibroblasts by IR, doxo, or
190 MiDAS and allowed 10 days for the senescent phenotype to develop as previously described
191 [10]. In parallel, the control cells were brought into quiescence state (Qui) by incubating in 0.2%
192 serum (minimal media) for 3 days by mock irradiation or treatment with DMSO in 0.2% serum
193 for 1 day. Senescence-induced cells and control cells (Qui or DMSO) were cultured in serum-
194 free medium for 1 day before collection of the conditioned media containing exosome SASP for
195 the mass spectrometric end-point analysis. Cell viability assays confirmed no detectable
196 difference in apoptosis/cell death in senescent and control fibroblast cells measured by
197 SYTOX™ Green Nucleic Acid Stain (Fig. S3A). Furthermore, EdU and SA-β-Gal counter staining

198 confirmed senescence (more than 90%) in IR-, doxo-, and MiDAS- induced senescent IMR90
199 cells compared to Qui control, while ~10% of senescent and Qui controls were dividing cells
200 (Fig. 3B). In MiDAS, mitochondrial dysfunction was observed by a decrease in NAD+/NADH
201 ratio indicating the electron transport chain was inhibited (Fig. S3B).

202 Size exclusion/ultrafiltration (SEC/UF)-enriched exosome proteins were extracted and
203 processed for label-free data-independent acquisition (DIA). The DIA-MS approach facilitated
204 sensitive and accurate quantification of exosome SASP proteins by quantification of the tandem
205 mass spectrometry (MS2) fragment ions, specifically quantifying the 'peak area under the curve'
206 from extracted ion chromatograms (XICs). We quantitatively compared exosome proteins (≥ 2
207 unique peptides) released by senescent fibroblasts with exosome proteins from Qui controls,
208 and we cataloged significantly changed proteins (q-value ≤ 0.05) that featured an absolute fold
209 change ≥ 1.5-fold (comparing senescent vs control) (Fig. 3C; Table S3A-F). Exosome proteins
210 were released at considerably higher levels by senescent fibroblasts compared to quiescent
211 control cells, and we refer to them as 'exosome SASP'. Our unbiased proteomic profiling
212 identified 1,426 exosome proteins amongst the three different senescent inducers, a large
213 fraction of which 60%, 48%, and 80% were significantly up- or down-regulated in IR, doxo, or
214 MiDAS, respectively (Fig. 3C). Interestingly, most of the significantly changed exosome proteins
215 (742) were markedly upregulated in the IR condition; in contrast, most exosome proteins (1,078)
216 were down-regulated in MiDAS-induced senescence (Fig. 3C). To visualize the significant
217 changes, the volcano plots of senescent fibroblasts versus Qui control (senescence/Qui)
218 showed the significantly altered protein levels (q-value ≤ 0.05, $|\log_2 \text{fold change}| \geq 0.58$) (Fig.
219 S3c, Table S3b, d, f). Up-regulated proteins in 'IR vs Qui' included Fermitin family homolog 3
220 (FERMT3), Creatine kinase M-type (CKM), Myosin-9 (MYH9) as well as numerous ribosomal
221 proteins (RPLs and RPs) and eukaryotic translation initiation factors (EIFs), while ECM proteins
222 collagens, laminins, Decorin (DCN), Biglycan (BGN), and nidogens were down-regulated. With
223 respect to 'Doxo vs Qui', up-regulation of several proteasome subunits (PSMCs, PSMDs,
224 PSME2), Protein VAC14 homolog (VAC14), and Collagen alpha-1(XII) chain (COL12A1), and
225 down-regulation of Endothelin receptor type B (EDNRB), Phospholipid phosphatase 3 (PLPP3),
226 Neuroblast differentiation-associated protein AHNAK were observed. 'MiDAS vs Qui'
227 comparison featured up-regulated Neutral amino acid transporter A (SLC1A4), complement

228 proteins and fibrinogens, and down-regulated Pantetheinase (VNN1), Procollagen C-
229 endopeptidase enhancer 1 (PCOLCE), collagens, and laminins. Although we discovered distinct
230 protein signatures per each of the senescence induction with proteins that are uniquely up- and
231 down-regulated with senescence, we also observed 318 exosome proteins that are common
232 between the different inductions (Fig. 3D). Specifically, we identified 46 up- and 103 down-
233 regulated exosome proteins that are common among the different senescence stimuli (Table
234 S3G and S3H, respectively). Top common up-regulated SASP proteins were Fermitin family
235 homolog 3 (FERM3), Creatine kinase M-type (CKM), Protein VAC14 homolog (VAC14), Neural
236 cell adhesion molecule 1 (NCAM1), and Tetraspanin-4 (TPS4). Top common down-regulated
237 proteins upon senescence induction included Procollagen C-endopeptidase enhancer 1
238 (PCOLCE), Endothelin receptor type B (EDNRB), Phospholipid phosphatase 3 (PLPP3),
239 Leukocyte elastase inhibitor (SERPINB1), and mitochondrial Superoxide dismutase [Mn]
240 (SOD2). The top up- and down-regulated exosome SASP proteins common between MiDAS,
241 doxo, and IR conditions are grouped into 12 biological processes (BP), such as cell adhesion,
242 proteolysis, and metabolism, and 5 cellular compartments (CC) (Fig. 3E); 72% of these common
243 proteins are known exosome (or EV) proteins. The clustering by partial least squares-
244 discriminant analysis (PLS-DA) confirmed distinct exosome profile clustering between
245 senescent fibroblasts and quiescent control fibroblasts, whereby clustering of senescent
246 conditions showed overlap in their exosome profiles (Fig. 3F). Furthermore, we compared our
247 IR-induced senescent fibroblast exosome proteins with the IR-induced soluble SASP from our
248 previous study by Basisty and Schilling et al. [10] and found 152 overlapping proteins, while 710
249 proteins were unique to the exosomes (EVs; Fig. 3G, Table S3I). Among the 152 common
250 proteins were identified Myosin-9 (MYH9), Growth/differentiation factor 15 (GDF15), Interstitial
251 collagenase (MMP1), C-type lectin domain family 11 member A (CLEC11A), and
252 Metalloproteinase inhibitor 1 (TIMP1), which were reported to associate with several traits of
253 aging and constitute a proteomic signature of aging [28, 29]. Exosome-specific proteins included
254 Clusterin (CLU), Serpin B5, dynactin subunits (DCTNs), numerous proteins related to DNA and
255 RNA metabolism (RNA helicase DDXs, heterogeneous nuclear ribonucleoproteins HNRNPs,
256 EIFs, RPs), proteasome subunits, and vacuolar protein sorting-associated proteins (VPSs). The
257 significantly altered senescent fibroblast exosome proteins identified in the study were
258 categorized based on subcellular locations: extracellular space (75%), membrane (72%),

259 exosome (70%), cytosol (56%), plasma membrane (38%), and cell surface (12%) (Fig. 3H). *In*
260 *silico* analysis of the significantly altered senescent exosome proteins identified 97 out of 1,340
261 proteins as surface proteins, of which 30 were consistent in all senescence stimuli (Fig. 3I, Table
262 S3J) and included Neural cell adhesion molecule 1 (NCAM1), A disintegrin and
263 metalloproteinase with thrombospondin motifs 13 (ADAMTS13), Neutral amino acid transporter
264 A (SLC1A4), and Tumor necrosis factor ligand superfamily member 4 (TNFSF4). These
265 upregulated senescent surface proteins have the potential to be developed into aging
266 biomarkers. Our proteomics data indicated a decrease in antioxidant proteins in senescent
267 exosomes compared to Qui controls, which is consistent with the higher intracellular oxidative
268 stress in senescent fibroblasts (Fig. 3J). Interestingly, MiDAS induction showed the most
269 elevated cellular oxidative stress, followed by doxorubicin (doxo) and irradiation (IR) as shown
270 in Fig. 3J.

271 **Plasma exosomes isolated from an aged human cohort display unique protein markers**

272 We performed a pilot study using human plasma samples from five young (20–26 years) and
273 five older individuals (65-74 years) (Table S1) to determine exosome-specific age signatures.
274 We used DIA-MS protein identification and quantification to analyze plasma exosomes from
275 young and elderly individuals and processed the data using our custom hybrid spectral library
276 (generated as described above) (Fig. S4). We reproducibly identified and quantified a total of
277 1,356 protein groups (≥ 2 unique peptides) (Table S4B)

278 Distinct and separate clustering of protein profiles from plasma exosomes from young and
279 old individuals were revealed by PLS-DA (Fig. 4A). Volcano plots of old versus young (old/young)
280 individuals showed 171 significantly altered exosome proteins (q-value ≤ 0.05, $|\log_2$fold change|
281 ≥ 0.58), of which 117 were down-regulated, whereas 54 were up-regulated in the older
282 individuals (Fig. 4B; Table S4C). A selection of key importance up- and down-regulated aging
283 plasma exosome proteins (26) are shown in Fig. 4C. Top up-regulated proteins included LIM
284 and SH3 domain protein 1 (LASP1), Hemopexin (HPX), Eosinophil peroxidase (EPX), Band 3
285 anion transport protein (SLC4A1), Leucine-rich alpha-2-glycoprotein (LRG1), as well as several
286 Serpins. Top down-regulated proteins were Calmodulin-like protein 5 (CALML5), Deoxyribose-
287 phosphate aldolase (DERA), Peroxidasin homolog (PXDN), Aminopeptidase N (ANPEP), and
288 Apolipoprotein L1 (APOL1). Out of them, 80% are classified as exosome proteins,

289 demonstrating the high yield and purity of the extracted plasma exosomes, and span nine
290 different biological processes, such as exocytosis, immune response, signal transduction, and
291 proteolysis (Fig. 4C).
292
293 To identify the biological relevance of our results, the differentially changing exosome
294 proteins in aging plasma from our DIA-MS analysis were integrated and highlighted using
295 ConsensusPathDB-human metabolic pathways and the Gene Ontology (GO) annotation
296 toolbox. Pathway enrichment analysis indicated remodeling in the plasma lipoprotein particles,
297 changes in blood coagulation, negative regulation of response to wounding, and reactive oxidant
298 activity – these pathways were significantly upregulated in plasma exosomes from older
299 individuals. Conversely, defense response to bacteria, acute inflammatory response, humoral
300 immune response regulation, cornification, and intermediate filament cytoskeleton organization
301 were pathways that were significantly down-regulated (Fig. 4D; Table S4J & S4K). The
302 significantly altered plasma exosome proteins identified in the study were categorized based on
303 subcellular locations: extracellular space (98%), membrane (64%), exosome (61%), plasma
304 membrane (42%), cytosol (42%), and cell surface (8%) (Fig. 4E). Individual changes in the
305 exosome protein level of Alpha-1-antitrypsin (SERPINA1) and Leucine-rich alpha-2-glycoprotein
306 (LRG1) positively correlated with older age (upregulation), whereas Apolipoprotein L1 (APOL1)
307 negatively correlated with age (downregulation) as shown in Fig. 4F, which further implies
308 distinct aging signatures in human plasma.
309
310 **Significant variations in lipid compositions of exosomes induced by different senescence**
311 **stimuli.**
312 In addition to exosome proteomics, we conducted a parallel lipidomic analysis of exosomes from
313 senescent fibroblasts induced by the three senescence-inducing stimuli. Exosomes enriched by
314 antibodies were subjected to lipidomic analysis using liquid chromatography ion mobility
315 separation collision-induced dissociation mass spectrometry (LC-IMS-CID-MS). By separating
316 lipids based on their LC retention time, IMS collision cross section (which is based on the lipid's
317 three-dimensional shape), and precursor and fragment ion masses, LC-IMS-CID-MS analyses
318 can reduce ambiguity and increase confidence in lipid identification and quantification. Here, we
319 quantitatively compared lipids from exosomes released from senescent and control fibroblasts

320 and cataloged significantly changed lipids (p_{adj}-value ≤ 0.05) that showed a fold change ≥ 2-fold
321 (senescent/control) (Fig. 5A; Table S5A). Lipidomic profiling revealed a substantial number of
322 statistically significant exosome lipids in response to the senescence inductions: with 122
323 regulated lipids with IR induction, 135 regulated lipids with doxo induction, and 129 regulated
324 lipids with MiDAS induction (yielding a total of 247 changed lipids upon senescence induction
325 considering all inducers). Notably, most of the significantly changed exosome lipids were
326 upregulated in all senescent conditions (Fig. 5A). Although there is variation in the lipids that
327 were up- and downregulated with senescence, 112 were shared amongst all inducers (Table
328 S5B and S5C). Furthermore, distinct clustering of senescent and control fibroblast exosome
329 profiles was revealed by PLS-DA (Fig. 5B). Individual lipid species profiles are further depicted
330 in the heatmap in Fig. 5C. Our results indicate that membrane lipids, such as phosphatidylcholine
331 (PC), phosphatidylethanolamine (PE), phosphatidylserine (PS), sphingomyelin (SM), and
332 hexosylceramide (HexCer) species were significantly upregulated in senescence conditions.
333 Specifically,top up-regulated lipids included PC(16:0_22:4), PC(18:0_24:0), PE(O-18:0/22:5),
334 PE(P-18:0/20:4), PS(18:1_22:0), SM(d18:2/16:0), HexCer(d18:1/24:0). Our analysis also
335 revealed senescence stimuli-specific changes in exosome lipids. Specifically, triglycerides (TG),
336 TG(16:0_18:1_20:4), TG(16:1_18:1_20:4);TG(18:2/18:2/18:2), and TG(54:6), and acylcarnitine
337 (AC) AC(18:0) species were downregulated with the doxo and IR inducers but not with MiDAS-
338 induced senescence (Fig. 5C). Additionally, specific PC and PC plasmalogen species (PC(P-)),
339 PC(P-18:0/20:5) and PC(P-16:0/22:5), were only upregulated with the MiDAS induction (Fig.
340 5C). Changes in the levels of specific exosome lipids such as PC (18:0_24:0) and SM
341 (d18:2/16:0) are further shown to illustrate they are positively correlated in all three senescent
342 conditions, while TG(54:6) is denoted for its decrease in only the doxo and IR inductions (Fig.
343 5D), suggesting unique senescence lipid signatures in human fibroblasts. Overall, these
344 significant changes in exosome-specific lipids highlight that they may play a potential role in the
345 senescence process.
346

347 **Exosomes miRNAs are differentially present in human plasma from young and older**
348 **individuals.**

349 To complement the exosome proteomic and lipidomic data, we performed in parallel a pilot
350 analysis of human plasma exosome miRNA cargo to identify differences between young (20–26

351 years) and older (65-74 years) individuals (Fig. 1). The length of miRNA sequences primarily
352 ranged from 18 to 24 nucleotides (Fig. S5a). In total, 1,375 miRNAs were identified from our
353 SEC/UF-extracted plasma exosomes (Table S6a), of which, 331 miRNA were consistent. 226
354 out of 331 miRNA were commonly shared between exosomes from both young and older
355 individuals, and 88 and 17 were unique to plasma exosomes from old and young individuals,
356 respectively (Fig. S5b; Table S6b). Volcano plots of old vs. young samples revealed six miRNAs
357 to be significantly altered. hsa-miR-27a-5p, -874-3p, PC-3p-73204_81, -3p-7719_599, and -3p-
358 8403_561 were upregulated, and hsa-miR-190a-5p was down-regulated in older individuals (Fig.
359 S5c; Table S6c), indicating that these miRNAs have a significant role in aging and could serve
360 as potential markers of aging. Pathway analysis of the six significantly altered miRNAs revealed
361 diverse pathways are associated with these miRNAs that could exacerbate underlying
362 mechanisms of aging (Fig. S5d). While it is not entirely clear what the function of these miRNAs
363 is it will remain of interest to monitor and report this important exosome cargo.
364

365 **Senescence and aging share mutual exosome signatures that may regulate age-related**
366 **inflammation and ECM remodeling, potentially causing secondary senescence.**

367 We demonstrate a substantial overlap between the exosome proteins identified (52) and altered
368 pathways between senescent fibroblasts and plasma from older individuals (Fig. 6B). Differential
369 profiles of selected exosome proteins in aging and senescence, such as Antithrombin-III
370 (SERPINC1), Prothrombin (F2), Coagulation factor V (F5), Plasminogen (PLG), Reelin (RELN),
371 Soluble scavenger receptor cysteine-rich domain-containing protein SSC5D, Complement C1
372 subcomponents (C1r and C1s), and HLA class I histocompatibility antigen, A-24 alpha chain
373 (HLA-A), showed complementary trends and were particularly associated with inflammation and
374 ECM remodeling (Fig. 6B). Our DIA-MS proteomics analysis of senescent fibroblasts identified
375 Plasminogen activator inhibitor 1 (SERPINE1), SPARC, Insulin-like growth factor-binding protein
376 7 (IGFBP7), Transforming growth factor beta-1 proprotein (TGFB1|1), and Integrin alpha-4
377 (ITGA4) as potential exosome protein candidates that can cause secondary senescence locally
378 and distally (Fig. 6A). Our lipidomics data revealed the presence of lipids such as hexceramides
379 HexCer(d18:1/24:0), HexCer(d18:1/24:1), and HexCer(d18:2/24:0), which induce secondary
380 senescence [30], and lysophosphatidylcholine (LPC) class lipids that are involved in ECM
381 modulation through metalloproteins. When comparing to the three different senescence-

382 inducing stimuli on IMR90 cells, we saw similarly affected pathways with human plasma
383 exosome aging. We observed a decrease in antioxidant and matrisome proteins, but more
384 interestingly changes in inflammatory and ECM-modifier associated proteins (Fig. 7), that play
385 crucial rolesin senescence. Dysregulation of the ECM composition, shape, firmness, and
386 abundance contribute to pathological conditions, such as fibrosis and invasive cancer.

387

388 **Discussion**

389 In recent years, several studies highlighted that the SASP secreted from senescent cells is highly
390 complex and very heterogeneous depending on tissue type, cell type and origin of senescence
391 or senescence induction [10, 31]. The composition of SASP can vary depending on a wide range
392 of factors, including cell type, senescence-inducing stimuli, and age. While there has been
393 significant progress in understanding SASP and its effect on neighboring cells and the
394 extracellular matrix, what is currently known is just the tip of the iceberg. Exosomes have been
395 recognized as a constituent of the SASP and are known to play a crucial role in facilitating
396 intercellular communication. Exosomes secreted from senescent cells are still relatively
397 underexplored. Understanding the complexity, cell-, tissue-, and stimuli-specificity of exosomes
398 from senescent cells could offer essential insights into the mechanisms underlying the
399 progression of senescence, aging, and age-related diseases. These insights could lead to the
400 development of potential diagnostic and therapeutic interventions.

401

402 We have laid out a comprehensive and quantitative DIA-MS proteomic workflow for
403 exploring exosome profiles from different senescence-inducing stimuli in cells and plasma.
404 Isolation and enrichment of intact and contamination-free exosomes are challenging, but we
405 propose that exosomes isolated by sequential SEC and UF improve the accuracy and reliability
406 of downstream proteomics analysis. This is based on specific sizes and surface markers that
407 distinguish exosomes from other extracellular vesicles and low levels of protein contaminants,
408 which can interfere with downstream analysis (Fig. 2). This approach led to the identification of
409 60-70% exosome-specific proteins in IMR90 fibroblasts (Fig. 3) and plasma (Fig. 4).

410

411 The limited availability of high-quality exosome libraries is another challenge. Spectral
412 library searching is a prerequisite for DIA quantitative proteomic analysis. We present three high-

413 quality human plasma exosome spectral libraries (DDA, directDIA, and hybrid), cataloging
414 around 2,700 high-confidence proteins as a resource for exosome proteomic research (Fig. S2).
415 The hybrid library identified a more considerable amount of total and significantly altered
416 proteins, while the directDIA approach is instrumental in cases where no pre-existing large
417 libraries are available, such as in non-model organisms or tissues. We emphasize the
418 significance of comprehensive quantitative workflows using DIA-MS proteomics for exosome
419 research. These mass spectrometric approaches offer highly robust workflows for biomarker
420 discovery in clinical samples, and specifically for biofluids and circulating biomarkers.
421
422 Previously we reported the profiling of soluble proteins and exosomes from senescent
423 cells and their SASP which led to the creation of the SASP Atlas [10]. Here we build on our prior
424 research by leveraging the DIA exosome proteomics workflow. This novel approach allowed us
425 to detect changes in the exosome protein profiles between young and old individuals in human
426 plasma, as well as from senescent IMR90 fibroblasts induced by IR, doxo, or MiDAS (Fig. 3).
427 Studying senescence and SASP with different senescent-inducing methods is essential to gain
428 a more comprehensive understanding of the SASP and identify commonalities and differences
429 in the composition, which can illuminate how the SASP components propagate and exacerbate
430 the senescent phenotype.
431
432 Our examination of SASP protein profiles in plasma samples from older individuals has
433 provided us with a more comprehensive understanding of the changes in intercellular
434 communication that occur with aging. This analysis encompasses exosomes derived from all
435 cell types, tissues, and senescence stimuli. In our study, we have identified 1,288 and 119
436 exosome-specific proteins unique to senescent fibroblasts and plasma samples from aging
437 cohorts respectively, while 52 proteins are common to both (Fig. 6B). By cross-analyzing
438 exosomes derived from plasma and cells, we could begin to dissect their endocrine and
439 paracrine mode-of-action in the context of senescence [4], which might potentially play a role in
440 secondary senescence. Johnson *et al.* (2020) conducted a meta-analysis of 36 proteomics
441 studies, identifying 818 aging-associated soluble proteins in the plasma proteome that were
442 altered in at least two studies [32]. Of these, 28 proteins overlapped with our age-associated
443 plasma exosome panel, 228 proteins overlapped with our exosome SASP components, and

notably, 14 proteins were common across all three datasets, as shown in Fig. S6 and Table S7. The limited overlap in proteins can be attributed to two main factors: first, we are comparing exosome SASPs and age-associated plasma exosome proteins with age-related soluble plasma proteins; second, our data were generated using mass spectrometry, whereas the Johnson *et al.* data were compiled from 36 studies using diverse proteomics methods.

Interestingly, several variants of immunoglobulins (n=61, as presented in Table S4c) show a strong negative correlation with aging. It suggests that the humoral immune response is downregulated in older individuals, which may contribute to the increased susceptibility to infections and diseases associated with aging (Fig. 4G). The downregulation of immunoglobulins in plasma exosomes from older individuals is consistent with previous studies that have reported age-related changes in the immune system, including a decline in B cell function and decreased antibody production. In contrast, SASP sustains and enhances inflammation, which is a broad immune response to tissue injury, infection, or other stimuli. While inflammation can be beneficial in response to acute infections or injuries, chronic inflammation can contribute to various age-related diseases. For example, exosomes released by prostate cancer cells carry pro-inflammatory M2 phenotype and promote a pro-tumorigenic microenvironment [33]. Here we demonstrate that the specific inflammatory proteins that are upregulated in the exosome SASP can vary depending on the senescence-inducing stimulus, but some common examples are serine protease inhibitors (SERPIN family, SERPINC1), Prothrombin (F2), Coagulation Factor V (F5), Reelin (RELN), Disintegrin and metalloproteinase with thrombospondin motifs 12 (ADAMTS12), Thrombospondin-1 (THBS1), Complement C3, and Complement C5 (Fig. 6-7). Further, we observed decreased levels of antioxidant proteins in senescent exosomes (Fig. 7). Biochemical analysis reveals an overall increase in intracellular oxidative stress in all senescent conditions, the highest being in MiDAS (Fig. 3J). Chronic oxidative stress and inflammation are closely linked and can lead to the development and progression of many age-related diseases, such as cancer, cardiovascular diseases, and neurodegenerative disorders [34]. In addition, inflammatory signals can degrade ECM components and alter the ECM structure [35].

Changes in the extracellular matrix (ECM) play a crucial role in senescence and cancer, as senescent cells alter the ECM by secreting ECM remodeling components. However, the

475 molecular understanding of the interplay between ECM and senescent cells is limited. Our study
476 revealed that exosomes secreted by senescent cells exhibit decreased level of ECM structural
477 proteins, including collagens, laminins, and Fibrillin-2 (Fig. 7). This suggests a potential
478 mechanism by which senescent cells destabilize the ECM, contributing to the propagation of a
479 senescent microenvironment. In addition, a decreased abundance in collagen mRNA levels is
480 noted in senescent retinal pigment epithelial cells, which are major ECM producers in the retina,
481 and hematopoietic stem cells [36]. ECM alterations are widely recognized as a significant factor
482 driving abnormal cellular responses [37], and recent research indicates that fragmentation of
483 collagen fibrils during aging leads to the disruption of fibroblast-ECM interactions [38]. This
484 disruption can contribute to the development of an "aged" phenotype. Our findings and those of
485 others strongly suggest that ECM and senescence play a critical role in aging.
486
487 Inflammation and ECM modulation might be two key factors contributing to secondary
488 senescence, leading to the accumulation of senescent cells and further promoting inflammation
489 and ECM remodeling. Recent studies suggest that sEVs can transfer senescent factors to non-
490 senescent/healthy cells [13, 39]. We identified multiple proteins, lipids, and miRNAs relevant to
491 paracrine senescence signaling that are upregulated in exosomes released by senescent
492 fibroblasts. Notable secondary signals include integrin alpha-4 [40], SERPINE1 [41, 42], insulin-
493 like growth factor-binding protein 7 [43, 44], transforming growth factor beta-1 proprotein [45],
494 SPARC [46], and hexceramides (HexCer) [30]. Additionally, miRNAs such as miR-483-5p [26],
495 miR-532-3p [26], and miR-409-3p [47] were consistently elevated. Our studies offer valuable
496 insights into the potential role of exosomes in SASP-mediated paracrine senescence, offering
497 potential therapeutic targets for mitigating its effects.
498 Our lipidomic analysis revealed consistent upregulation of phospholipid classes, including
499 phosphatidylcholine (PC) and phosphatidylethanolamine (PE), aligning with previous studies in
500 senescent cells [48]. Furthermore, we observed significant increases in PS, SM, and ether-
501 linked/plasmalogen PE species (PE(O/P-)) across all senescence inducers, implicating altered
502 exosomal lipid composition in senescence-associated changes in cellular functions, particularly
503 membrane dynamics. Conversely, lower levels of specific triglycerides (TG) and acylcarnitines
504 (AC) were noted, except in MiDAS-induced senescence, possibly reflecting reduced TG
505 accumulation [49] and decreased AC synthesis during senescence. Finally, while 112 lipids were

506 commonly altered across all senescence inducers, distinct lipid signatures were observed for
507 specific stimuli, such as doxo (7 unique lipids) and MiDAS (9 unique lipids; Table S5c),
508 highlighting stimulus-specific molecular mechanisms of senescence. These findings deepen our
509 understanding of exosome-mediated signaling in senescence and point toward tailored
510 approaches for therapeutic intervention.

511 Increasing evidence of age-associated changes in miRNA levels is seen in various
512 models, ranging from nematodes to humans [38]. We reproducibly identified 88 unique miRNAs,
513 including miR-27a-5p, -874-3p, in plasma exosomes from older individuals. An upregulation of
514 miR-27a is reported in degenerative diseases such as osteoarthritis [50] and AD [51]. Moreover,
515 miR-874 was identified in circulating brain fluid from patients with mild cognitive impairment [52]
516 and as a biomarker for early AD development [52, 53]. These miRNAs could be developed into
517 future senescence biomarkers. Further investigations within larger aging populations and
518 longitudinal analysis are needed to confirm the potential of these protein, lipid, miRNA candidate
519 signatures as diagnostic and prognostic biomarkers.

520

521 Overall, we describe an exosome DIA-proteomic and multi-omic workflow for exploring exosome
522 profiles from cells and plasma. We emphasize the power and potential of using DIA-MS
523 proteomic data analysis for exosome research as a highly robust workflow for biomarker
524 discovery in clinical samples. Our study reveals that the exosome SASPs exhibit considerable
525 heterogeneity, and we systematically report the changes in exosome cargo, specifically proteins,
526 lipids, and miRNAs, between young and old individuals and senescent fibroblasts induced by
527 IR, doxo, or MiDAS. We also report that exosomes may be critical players in mitigating
528 senescence and aging by inflammation, oxidative stress, ECM modulation, and secondary
529 senescence. Additional investigations and functional validations are required to ascertain the
530 mechanisms by which exosomes mediate their effects in the context of senescence and aging
531 and understand how the senescence- and age-associated exosome cargos can impact the
532 recipient cells. This can help understand the global molecular mechanisms underlying aging and
533 age-related diseases and potentially identify novel therapeutic targets or biomarkers to target
534 and regulate senescent cell-secreted exosomes or use them as therapeutic agents.

535

536

537 **Methods**

538 **Human Plasma Samples.**

539 We obtained 10 plasma samples, 5 from young individuals (20-26 years old) and 5 from older
540 individuals (65-74 years old), with no restrictions regarding gender, from the Blood Centers of the
541 Pacific in San Francisco, CA, detailed in Table S1. Specimens from individuals with any known
542 autoimmune disorders, chronic diseases, bleeding disorders, or neurodegenerative disorders were
543 excluded. The plasma samples were aliquoted and stored at -80°C until further use. IRB approvals
544 were not required for the plasma samples.

545

546 **Primary human fibroblast tissue culture and senescence induction**

547 **(a) Primary human fibroblast tissue culture**

548 Primary human lung fibroblasts (IMR-90) used in the study were acquired from ATCC, Manassas,
549 VA (#CCL-186). Cells were maintained in Dulbecco's Modified Eagle Medium (DMEM)
550 supplemented with penicillin and streptomycin (5,000 U/mL and 5,000 µg/mL; Thermo Fisher
551 Scientific, Waltham, MA, #15070063) and 10% fetal bovine serum (FBS; Thermo Fisher Scientific,
552 Waltham, MA, #2614079), and incubated at 37°C in an atmosphere of 10% CO_2 and 3% O_2.

553

554 **(b) Senescence induction in primary human fibroblasts**

555 Irradiation (IR), doxorubicin (doxo), and Antimycin A induced-mitochondrial dysfunction-associated
556 senescence (MiDAS) were used to induce senescence in IMR90 cells. For IR induction, the cells
557 were irradiated with ionizing radiation (10 Gy) for 30 minutes. For doxo induction, the cells were
558 treated with 350 nM doxo (Thermo Scientific #25316-40-9) for 24 h. For MiDAS induction, 200 µM
559 Antimycin A (AA; Thermo Scientific # 1397-94-0) was supplemented to the complete media every
560 alternate day for 10 d. After senescence induction, the cells were cultured for 10 d to allow the
561 senescent phenotype to develop. The conditioned media was collected for exosome analysis after
562 the cells were washed with phosphate-buffered saline (PBS; Gibco™ #10010023) and placed in
563 serum- and phenol-red-free DMEM media for 24 h. In parallel, the control cells were made
564 quiescent by incubating in 0.2% serum (minimal media) for 3 d by mock irradiation or treated with
565 DMSO in 0.2% serum for 1 d. Subsequently, senescence-induced and control fibroblasts were
566 placed in serum- and phenol-red-free DMEM media for 24 h before collecting the conditioned media
567 for exosome analysis.

568

569 **(c) Cell viability assays**

570 On day 10 for senescence-inducers or day 3 for control quiescent cells (as shown in Fig. 3A (ii)),
571 cell viability was assessed using SYTOX Green (Invitrogen, Carlsbad, CA, #S7020). The protocol
572 recommended by the manufacturer was followed, which involved staining the cells with SYTOX,
573 and counting the nuclei that exhibited staining to indicate cell death using a fluorescent microscope
574 (Evident, #Olympus IX70 Fluorescence) with a wavelength of 523 nm.

575

576 **(d) EdU and SA-β-Gal staining**

577 The activity of SA-β-gal (senescence-associated β-galactosidase) was determined using a
578 BioVision Senescence Detection Kit (Milpitas, CA, #K320-250), which is specifically designed to
579 measure the activity of lysosomal β-galactosidase enzyme that is known to increase significantly
580 in senescent cells. To perform the assay, 7000 cells for each condition, including replicates, were
581 seeded into 8-well culture slides coated with poly-lysine (Corning, Corning, NY; #354632). After 24
582 h, the cells were stained with the SA-β-gal detection reagent according to the manufacturer's
583 protocol. In addition to measuring SA-β-gal, we evaluated cell proliferation using the Click-iT EdU
584 Cell Proliferation Assay Kit (Invitrogen, #C10337). This kit utilizes a thymidine analog, EdU, which
585 is incorporated into newly synthesized DNA during the S-phase of the cell cycle. The cells were
586 treated with 10 μM EdU for 24 h, then fixed and permeabilized. The incorporated EdU was detected
587 using a Click-iT reaction cocktail that binds to the EdU and produces a fluorescent signal. The EdU
588 and SA-β-Gal stained cells were then imaged using a Fluorescence microscope (Olympus USA, #
589 IX70) and quantified using Image J software (IJ 1.46r, NIH). Overall, EdU and SA-β-Gal assays
590 allow for measuring both senescence and cell proliferation in response to different senescence-
591 induction.

592

593 **(c) NAD+/NADH ratio determinations**

594 We measured NAD+ and NADH levels of Antimycin A-treated MiDAS-induced senescent, and Qui
595 control IMR90 cells using a commercial colorimetric NAD/NADH Assay Kit (Abcam, UK,
596 #ab65348). The assays were performed in biological triplicate, with 2 X 10^6 IMR90 cells lysed in
597 NAD/NADH extraction buffer by two freeze/thaw cycles (20 minutes on dry ice followed by 10
598 minutes at RT), followed by centrifugation (14,000 X g for 5 min at 4°C) and filtration (10 kDa cut-

599 off filters, MilliporeSigma™, #UFC501024) to remove cellular debris and proteins. The resulting
600 supernatant was then subjected to a series of enzymatic reactions that converted NADH to a
601 fluorescent product (absorbance at 450 nm) as per the manufacturer's instructions, allowing for
602 quantitative measurement of the NAD+/NADH ratio.
603
604 **(d) Oxidative stress measurements**
605 Lipid peroxidation is a common consequence of oxidative stress. A lipid peroxidation assay kit
606 (Abcam, UK, #ab233471) was used to measure cellular oxidative stress in IR-, doxo-, and MiDAS-
607 induced senescent fibroblasts. Qui or DMSO fibroblasts were used as a control for comparison.
608 Briefly, 5 X 10^5 cells in triplicates for each condition were homogenized in 500 µL of 20mM Na
609 Phosphate buffer (pH about 3 to 3.2) and 0.5% TritonX-100 to solubilize the cell membranes,
610 followed by centrifugation (14,000 X g for 5 min at 4°C) to remove cellular debris. The resulting
611 supernatant was then subjected to a series of chemical reactions per the manufacturer's
612 instructions to produce a colored product, which was quantified spectrophotometrically at 695 nm.
613
614 **Exosome isolation and enrichment**
615 **(a) Human plasma**
616 Ultracentrifugation (UC), sequential SEC coupled with either ultrafiltration (SEC/UF) or
617 ultracentrifugation (SEC/UC) was used to isolate and enrich exosomes from plasma. Plasma was
618 centrifuged at 3,000 x g for 10 min to remove cellular debris and then centrifuged at 10,000 x g for
619 10 min to remove apoptotic cell bodies. The supernatant (2 mL) containing extracellular vesicles
620 was then proceeded by UC, SEC/UF, or SEC/UC.
621
622 For SEC, the supernatant was passed through a qEV size-exclusion column (Izon, #qEV35)
623 for exosome enrichment, according to the manufacturer's instructions. Briefly, the column was
624 maintained at room temperature for 20 min before use and then activated by flushing with 1.5x
625 column volume of degassed PBS (~60 mL). The supernatant was passed through the activated
626 qEV size exclusion columns (by gravity drip). Different fractions were collected by filling the
627 reservoir with PBS (~50 mL). The initial 14 mL of flow-through was void volume, while the
628 subsequent 10 mL (collected in 5 x 2 mL centrifuge tubes: labeled as E1–5) was enriched exosome
629 fractions based on immuno-blotting with exosome-specific protein markers (Fig. 2). The remaining

630 26 mL was marked as the post-exosome fractions that contained plasma proteins. qEV size-
631 exclusion exosome fraction (E1–5) were quality-checked spectrophotometrically (SpectraMax Plus
632 384, Molecular devices), where OD600 was used for exosome quantification and OD280 for
633 plasma proteins. Based on higher plasma protein contamination in fraction E5, we pooled only
634 fractions E1–E4 to obtain highly pure exosomes. Subsequently, fractions E1–E4 were
635 concentrated by ultrafiltration (UF; Amicon® Ultra 50 kDa, # UFC903024) or ultracentrifugation
636 (Optima, The Beckman Coulter Life Sciences) for further exosome analysis.
637

638 **(b) DMEM-conditioned media**

639 50 mL of conditioned media from IR, doxo, MiDAS-senescent, and Qui-control IMR90 cells were
640 centrifuged at 3,000 x g for 10 min to remove any cell debris. The supernatant was passed through
641 a 50 kDa cut-off filter. PBS was added to the remaining filtrate to make up to 2 mL. The filtrate was
642 then centrifuged at 15,000 x g for 30 min to remove apoptotic cell bodies and proceeded with either
643 SEC/UF or Antibody-based extractions (AbE). For SEC/UF, the supernatant was passed through
644 a size exclusion chromatography column followed by ultrafiltration to enrich and purify the
645 exosomes, as described previously.

646 For AbE enrichment a Miltenyi Biotec exosome isolation kit (Miltenyi Biotec, #130-110-912)
647 was used to label the exosomes with magnetic microbeads that specifically bind to exosome
648 surface markers. Briefly, 2 mL of filtrate was added to 50 µL of magnetic microbeads and incubated
649 for 1 h at room temperature on a rotor. A micro-column was equilibrated with 100 µL of equilibration
650 buffer and washed thrice with 100 µL of isolation buffer. The labeled exosomes were then passed
651 through a micro-column, and the exosomes were selectively retained on the column while other
652 non-exosome particles were removed. Finally, the exosomes were washed 4x with 100 µL isolation
653 buffer and eluted with 200 µL of elution buffer. We used SEC/UF for proteomics analysis, while
654 AbE was used for lipidomics studies.
655

656 **Exosome quality check**

657 **(a) Size distribution analysis**

658 Exosome diameter was assessed by tunable resistive pulse sensing (TRPS) on an IZON qNano
659 Gold nanoparticle characterization instrument using an NP150 nanopore membrane at calibration

660 with 110-nm carboxylated polystyrene beads at a concentration of 1 × 10^{10} particles/mL (Zen-bio,
661 Research Triangle, NC).
662
663 **(b) Immunoblotting**
664 Exosomes were lysed in RIPA buffer (Thermo Scientific™, #89900) for protein extraction. Exosome
665 proteins were quantified using BCA (Thermo Scientific™, #23225). 20 µg of protein/well was
666 separated on 12% SDS-PAGE and transferred onto PVDF membranes under semi-dry conditions
667 using the Trans-Blot Turbo Transfer System transfer unit (Bio-Rad, #1704150). Ponceau S staining
668 (Sigma-Aldrich, #P7170-1L) confirmed equal loading of exosomal proteins. Immunoblotting was
669 performed using 1:1000 dilution of CD9 (Abcam, #Ab96696), Tumor susceptibility gene 101
670 (TSG101, Santa Cruz Biotechnology, #sc-7964), albumin (Abcam, #Ab106582), or Immunoglobulin
671 G (IgG, Abcam, #Ab200699), and anti-rabbit HRP-conjugated antibody (Bio-Rad, #1706515) or
672 anti-mouse HRP-conjugated antibody (Abcam, #Ab6728) as a secondary antibody (1:3000
673 dilution). Blots were developed per the manufacturer's protocol with the Pierce ECL Western
674 Blotting Substrate (Thermo Fisher Scientific, #32106). Imaging was performed by Azure
675 Biosystems c600. Densitometric analysis of bands was performed using Image J software (IJ 1.46r;
676 NIH).
677
678 **Mass spectrometric analysis of exosome proteins**
679 **(a) Protein extraction and trypsin digestion**
680 Plasma exosomes were lysed in lysis buffer (8 M urea, 0.1 M ammonium bicarbonate), and then
681 reduced by 10 mM tris(2-carboxyethyl) phosphine (TCEP) and alkylated using 40 mM
682 chloroacetamide (CAA) for 1 h at 37°C. The solution was diluted with 0.1 M ammonium bicarbonate
683 buffer to lower the urea concentration to 1.5 M and digested with trypsin (Promega, Madison, WI,
684 # V5111) at a 1:100 ratio (protease to protein (wt/wt)) overnight at 37°C. Peptides were purified
685 using MacroSpin clean-up columns (NEST group, Southborough, MA, # SEM SS18V), following
686 the manufacturer's protocol. Eluted peptides were vacuum dried and then resuspended in 60 µL of
687 1% acetonitrile acidified with 0.1% formic acid buffer spiked with iRT peptides (Biognosys,
688 Schlieren, Switzerland, # Ki-3002-1). Peptides were quantified using nano-drop (Spectrostar Nano,
689 BMG Labtech, # UV5Nano) and adjusted to a 1 mg/mL concentration.
690

691 IMR90 cell exosomes were lysed in the lysis buffer (5% SDS and 50 mM TEAB), reduced,
692 alkylated, and acidified to a final concentration of 1.2% phosphoric acid. Then 90% methanol in
693 100 mM TEAB was added and passed through micro S-Trap columns (Protifi, #C02-micro-80).
694 IMR90 exosome proteins trapped in the S-Trap columns were digested with trypsin (Promega,
695 Madison, WI, # V5111) in digestion buffer (50 mM TEAB, pH ~8) at a 1:25 ratio (protease to protein
696 (wt/wt)) overnight. Peptides were eluted from the S-Trap column with 50 mM TEAB and 0.5% formic
697 acid and then with 50% acetonitrile in 0.5% formic acid. Pooled elution solutions were dried in a
698 speed vac and resuspended in 0.2% formic acid. The resuspended peptide samples were desalted,
699 concentrated, and resuspended in aqueous 0.2% formic acid containing 'Hyper Reaction
700 Monitoring' indexed retention time peptide standards (iRT, Biognosys, #Ki-3002-1).
701
702 **(b) Reversed-phase fractionation (RP) for deep spectral library generation**
703 For DDA library generation, 400 µg of plasma exosome peptides (pooled from 10 different plasma
704 exosome samples) were injected onto Dionex Ultimate 3000 LC (Thermo Scientific) coupled to
705 ACQUITY UPLC CSH1.7 mm C_{18} column (2.1 x 150 mm) (Waters, Milford) for fractionation using
706 RP. Peptides were chromatographically separated in a 30-min non-linear gradient from 1% to 40%
707 RP buffers (Buffer B: 100% ACN; Buffer A: 20 mM ammonium formate, pH 10). A micro fraction
708 was taken every 45 seconds, pooled into 24 final peptide fractions, vacuum dried, resuspended in
709 20 mL buffer A spiked with iRT peptides, and quantified. Each fraction was acquired in DDA mode,
710 as described below.
711
712 **(c) LC-HCD-MS-based exosome proteins data acquisition**
713 2 µg of trypsin-digested plasma exosome peptides were separated using liquid chromatography
714 coupled to a mass spectrometer. The analytical column was in-house packed into a fritted tip
715 emitter to a length of 50 cm (ID 75 µm) (New Objective, Woburn, MA) using the CSH C_{18} phase
716 (1.7 µm) (Waters, Milford, MA). The column was operated using an Easy nLC 1200 (Thermo Fisher
717 Scientific, San Jose, CA) coupled online to an Exploris 480 spectrometer (Thermo Fisher
718 Scientific). Peptides were eluted at 250 mL min-1 using a non-linear 2-h gradient from 1% to 45%
719 buffer B (Buffer B: 80% ACN + 0.1% FA; Buffer A: 0.1% FA). Based on the RP samples, the mass
720 spectrometer was operated in a data-dependent mode for DDA library generation. Briefly, the
721 following settings were applied: MS1 scan resolution: 60,000; MS1 AGC target: 300; MS1

722 maximum IT: 25 ms; MS1 scan range: 350–1650 Th; MS2 scan resolution: 15,000; MS2 AGC
723 target: 200; MS2 maximum IT: 25 ms; isolation window: 4 Th; first fixed mass: 200 Th; NCE: 27;
724 minimum AGC target: 1e3; only charge states 2 to 6 considered; peptide match: preferred; dynamic
725 exclusion time: 30 s.

726 In DIA mode, all samples were acquired in a randomized fashion with regard to the different
727 conditions: young and old. The mass spectrometer was operated using the following parameters
728 for the MS1 scan: scan range: 350 to 1650 Th; AGC target: 300%; max injection time: 20 ms; scan
729 resolution: 120,000. The MS1 was followed by targeted MS2 scan events with the following
730 settings: AGC target: 1000%; max injection time: 54 ms; scan resolution: 30,000; scan range: 350-
731 1,650 m/z Th; normalized collision energy: 27. The number of DIA segments and the segment
732 widths were adjusted to the precursor density and to achieve optimal data points across each peak
733 for each acquisition (Table S8a). The DIA methods consisted of 40 DIA segments with a cycle time
734 of 3.2 s.

735 IMR-90 exosome peptides were separated on a Dionex UltiMate 3000 system, and DIA-MS
736 acquisition was performed on an Orbitrap Eclipse Tribrid mass spectrometer (Thermo Fisher
737 Scientific, San Jose, CA). The solvent system consisted of 2% ACN, 0.1% FA in H2O (solvent A),
738 and 98% ACN, 0.1% FA in H2O (solvent B). Proteolytic peptides (50 ng) were loaded onto an
739 Acclaim PepMap 100 C_{18} trap column (0.1 x 20 mm, 5 µm particle size; Thermo Fisher Scientific)
740 for 5 min at 5 µL/min with 100% solvent A. Peptides were eluted on an Acclaim PepMap 100 C_{18}
741 analytical column (75 µm x 50 cm, 3 µm particle size; Thermo Fisher Scientific) at 300 nL/min using
742 the following gradient of solvent B: 2% for 5 min, linear from 2% to 20% in 125 min, linear from
743 20% to 32% in 40 min, up to 80% in 1 min, 80% for 9 min, down to 2% in 1 min, and 2% for 29 min,
744 for a total gradient length of 210 min. Full MS spectra were collected at 120,000 resolution (AGC
745 target: 3e6 ions, maximum injection time: 60 ms, 350-1,650 m/z), and MS2 spectra at 30,000
746 resolution (AGC target: 3e6 ions, maximum injection time: Auto, NCE: 27, fixed first mass 200 m/z).
747 The isolation scheme consisted of 26 variable windows covering the 350-1,650 m/z range with an
748 overlap of 1 m/z (Table S8b) [54].

749

750 **(d) Exosome protein spectral library generation from DDA and DIA**

751 Three spectral libraries were generated i) a deep DDA-based spectral library, ii) a DIA-only spectral
752 library (directDIA), and iii) a hybrid spectral library (hybrid) (Fig. 1). The DDA deep spectral library

753 was generated by performing DDA analysis on 25 RP fractions representing fractions from a pooled
754 mixture of peptides obtained from the same 10 plasma exosome protein samples (n = 5, young
755 and old each). DDA raw files (n = 25) were individually searched with Pulsar in Spectronaut version
756 14.0.200601.47784 (Biognosys) against the Human UniProt FASTA (downloaded on January 31,
757 2018, containing 92,931 proteins) using the following settings: fixed modification: carbamidomethyl
758 (C); variable modifications: acetyl (protein N term), oxidation (M); enzyme: trypsin/P with up to two
759 missed cleavages. Spectronaut automatically determined mass tolerances and other settings were
760 set to default. Search results were filtered using a 1% false discovery rate on the precursor ion,
761 peptide, and protein levels [55, 56]. For the directDIA spectral library, 10 individual DIA acquisitions
762 of plasma exosomes (n = 5, young and old each) were processed using Pulsar in Spectronaut
763 version 14.0.200601.47784 using the same human FASTA file and settings as above. We
764 combined both DDA and directDIA libraries for the hybrid library generation in Spectronaut. All
765 Spectronaut parameter settings were uploaded to the data repository.
766
767 **(e) DIA data processing and quantification**
768 Quantitative analysis was performed by processing protein peak areas determined by the
769 Spectronaut software. Prior to library-based analysis of the DIA data, the DIA raw files were
770 converted into htrms files using the htrms converter (Biognosys). MS1 and MS2 data were
771 centroided during conversion, and the other parameters were set to default. For the human plasma
772 exosome cohort, the htrms files were analyzed with Spectronaut (version: 14.0.200601.47784,
773 Biognosys) using the previously generated libraries to perform quantitative data analysis with the
774 three libraries generated (see above): the directDIA library, the deep DDA spectral library, and the
775 hybrid library. Briefly, calibration was set to non-linear iRT calibration with precision iRT selected.
776 DIA data was matched against the described spectral library supplemented with decoys (library
777 size fraction of 0.1) using dynamic mass tolerances. Quantification was based on MS/MS XICs of
778 3-6 MS/MS fragment ions, typically y- and b-ions, matching specific peptides in the spectral library.
779 Interference correction was enabled on MS1 and MS2 levels. Precursor and protein identifications
780 were filtered to 1% FDR, estimated using the mProphet algorithm, and iRT profiling was enabled.
781 Quantification was normalized to the local total ion chromatogram. Exosome proteins identified
782 with less than two unique peptides were excluded from the analysis. The DIA data was processed
783 for relative quantification comparing peptide peak areas from different conditions (old vs. young

784 plasma and senescent vs. Qui control IMR90 fibroblasts). Differential analysis was performed
785 applying paired t-test, and p-values were corrected for multiple testing. Protein groups with q-value
786 ≤ 0.05 and $\log_2$ ratio ≥ 0.58 were considered significant. For the IMR90 exosome cohort, DIA data
787 were analyzed with Spectronaut (version: 15.1.210713.50606, Biognosys) without a spectral library
788 using the directDIA algorithm. Similar settings were applied for DIA data processing and differential
789 analysis.
790
791 **Mass spectrometric exosome lipid analysis**
792 **(a) Exosome lipid extraction**
793 AbE-based enriched exosome lipids were extracted by a modified Folch extraction method [57,
794 58]. Briefly, 200 µL of fibroblast (IMR-90) exosomes in methanol were also transferred into a 1.7
795 mL Sorenson microcentrifuge tube (# 89082-332) for lipid extraction. The IMR90 cell exosome
796 count ranged from 10-13 million and was used for IMR90 sample normalization. Each IMR90
797 exosome sample (200 µL) was initially diluted in 200 µL in Optima LC-MS grade methanol, where
798 the IMR90 cell exosomes were normalized to 10 million exosomes present. Each sample was dried
799 in a Thermo Scientific Speedvac SPD130DLX (San Jose, CA) for 30 min, and then 750 µL of chilled
800 methanol was added to each tube. The samples were then transferred to a 2.0 mL bead tube that
801 contained 2.4 mm tungsten carbide beads (Fisher Scientific, #15-340-153) before being placed
802 into a Fisher Brand Bead Mill 24 Homogenizer (#15-340-163) for 2 min at a frequency of 30 Hz for
803 2 cycles. Each sample was then placed into a 5.0 mL glass vial (Fisher Scientific, #S28023)
804 equipped with a Teflon-lined cap, and 750 µL of methanol was added. Next, 3.0 mL of chloroform
805 (Sigma Aldrich LC-MS grade) and 200 µL of ultrapure water (Optima LC-MS grade) were added to
806 induce phase separation. Samples were then vortexed with a VWR Standard Heavy-Duty Vortex
807 Mixer for 30 s before being placed in a Branson CPX5800H sonicator for 30 min at room
808 temperature. Once completed, the samples were incubated at 4°C for 1 h to achieve the phase
809 separation. For each sample, 1.20 mL of water was added, and mixed gently. Next, the samples
810 were placed in an Eppendorf 5810R Centrifuge and centrifuged at 1000 rpm for 10 min. Finally,
811 300 µL of the bottom organic layer of each sample was collected and dried in a speed vac for
812 approximately 40 min until dry. The total lipid extracts were finally reconstituted with 190 µL of
813 methanol and 10 µL of chloroform and stored at -20°C until mass spectrometric analyses were

814 conducted the following week. Before mass spectrometric measurements, stored samples were
815 dried and reconstituted in the 190 µL:10 µL methanol:chloroform solvent mixture.
816
817 **(b) LC-IMS-CID-MS-based exosome lipids data acquisition**
818 An Agilent 1290 Infinity II UHPLC (Santa Clara, CA) coupled with an Agilent 6560 IM-QTOF mass
819 spectrometer (Santa Clara, CA) was used for the LC-IMS-CID-MS analysis of IMR90 exosome
820 lipids [59]. For the exosome lipid acquisition, 10 µL of extracted exosome lipids were injected onto
821 a reversed-phase Waters CSH column (3.0 mm x 150 mm x 1.7 µm particle size) and
822 chromatographically separated over a 34 min gradient period (Mobile Phase A: 10 mM NH_4AC in
823 ACN/H_2O (40:60); Mobile Phase B: 10 mM NH_4 ACN/IPA (10:90)) at a flow rate of 250 µL/min [60].
824 Details regarding the gradient and column wash are provided in Table S8c. Lipids were
825 subsequently analyzed using positive and negative ionization modes using an Agilent Jet Stream
826 ESI source (Agilent Technologies, Santa Clara, CA). The lipids were focused, trapped, and pulsed
827 into the IMS drift cell using a high-pressure and trapping ion funnel with pressures ~4 torrs [59].
828 Ions were then separated with drift tube IMS (DTIMS) in the 78 cm drift tube following the ion funnel.
829 Ions were then transferred to a hexapole collision cell where alternating precursor and all-ions
830 fragmentation scans were acquired. Collision energies for the collision-induced dissociation (CID)
831 analyses were ramped based on the various IMS drift times for the different lipid species of interest,
832 providing optimized fragmentation for the varying ion sizes as well as 1+ and 1- charge states [61].
833 The collision energy ramp applied based on IMS drift time is shown in Table S8d. Finally, various
834 ion optics transferred the ions to the time-of-flight (TOF) mass spectrometer. The TOF mass
835 spectrometer was set to evaluate a mass range of 50 to 1700 *m/z,* and the LC, IMS, and MS
836 information were collected in an Agilent .d file. Brain total lipid extract (BTLE; Avanti Polar Lipids,
837 Alabaster, AL #131101C) was used as quality control (QC) for the LC, IMS, and MS values and
838 observed peak abundances.
839
840 **(c) Lipid Identification**
841 For lipid identification, we considered LC retention times, IMS collisional cross section (CCS), and
842 m/z values of the precursor and fragment ions with Skyline software and a lipidomic plasma library
843 comprising 516 unique lipids published previously [62]. These lipids were all experimentally
844 validated with LC, IMS, and MS information. Speciation of the lipids included the headgroup and

845 fatty acyl (FA) components (e.g., PE (16:0_18:0)) but did not account for double bond position and
846 orientation or specific backbone position. A total of 247 exosome lipids were identified in all
847 samples (Table S5a).
848
849 For the lipidomic comparative analysis, the lipid intensities were total ion chromatogram (TIC)
850 normalized and log_2 transformed. To assess clustering, PLS-DA was performed using the
851 package 'mixOmics'. Significant lipids were identified in R using the package 'limma', which
852 employs linear models to assess differential expression in complex experiments. The resulting
853 p-values were adjusted using Benjamini-Hochberg correction and fold changes were log_2
854 transformed. A heatmap of significant lipids was created using the package 'pheatmap' and
855 group clustering was assessed using Euclidean distance and complete linkage. Finally, violin
856 plots were created using the package 'ggplot2'. The exported statistical outputs, including log_2
857 fold changes and p-values for the IR vs. LSM (Qui), doxo vs. DMSO, and MiDAS vs. DMSO
858 comparisons are provided in Tables S5b and S5c.
859
860 **Plasma exosome miRNA extraction, deep sequencing, and analysis**
861 The SEC/UF extracted plasma exosomes were outsourced to LC Sciences, LLC (Houston, TX) for
862 miRNA deep sequencing and analysis. Briefly, a small RNA (sRNA) library was generated for 10
863 plasma exosome samples (n=5, young and old individuals each) using a propriety Illumina
864 Truseq™ Small RNA Preparation kit (Illumina, # RS-930), according to the manufacturers' guide.
865 The purified cDNA library was used for cluster generation on Illumina's Cluster Station and then
866 sequenced on Illumina GAIIx following the vendor's instruction for operating the instrument. Raw
867 sequencing reads (40 nts) was obtained using Illumina's Sequencing Control Studio software
868 version 2.8 (SCS v2.8), following real-time sequencing image analysis and base-calling by
869 Illumina's Real-Time Analysis version 1.8.70 (RTA v1.8.70). The extracted sequencing reads were
870 used in the standard data analysis. A proprietary pipeline script, ACGT101-miR v4.2 (LC Sciences),
871 was used for sequencing data analysis [63]. For the miRNA differential analysis, a p-value < 0.05,
872 an absolute fold change > 1.5, and a read count > 0 in each condition were required to identify
873 statistically-significant changes.
874
875

876 **Data availability**

877 **a. Exosome protein cargo**

878 All mass spectrometry raw files, spectral libraries, Spectronaut files, descriptive methods, and other
879 supplementary tables and data have been deposited to MassIVE
880 ftp://MSV000086782@massive.ucsd.edu under MSV000086782 and ProteomeXchange under
881 PXD023897 (http://proteomecentral.proteomexchange.org). The Spectronaut projects that are
882 uploaded to the repositories can be viewed using the free Spectronaut viewer
883 (www.biognosys.com/technology/spectronaut-viewer).

884 **b. Exosome lipid cargo**

885 All mass spectrometry raw files and datasets have been deposited to MassIVE
886 ftp://massive.ucsd.edu/v07/MSV000094326/ under MSV000094326.

887

888 **Statistical analysis**

889 Five biological replicates were analyzed for exosome plasma studies and four biological replicates
890 for the senescent fibroblasts IMR90 studies. We used the two-tailed Student's t-test or ANOVA
891 (GraphPad Prism, La Jolla, CA, USA) to determine differences between the groups. Unless stated
892 otherwise, the experimental data are presented as the mean ± standard deviation (SD) from three
893 independent experiments.

894

895 **Pathway and network analysis**

896 We conducted gene set over-representation analyses using the ConsensusPathDB-human tool,
897 release 34 (15.01.2019). Specifically, we analyzed a list of all proteins that were significantly
898 increased or decreased (q-value < 0.05) in (a) Old vs. young plasma, (b) IR vs. Qui, (c) doxo vs.
899 Qui, and (d) MiDAS vs. Qui. We referenced curated pathways for enrichment analysis from the
900 Gene Ontology (GO) Database, focusing on "Biological Process" term categories. We considered
901 pathways with a minimum of three observed proteins, q-value < 0.01, and GO terms restricted to
902 levels 4–5 as significant. To provide background reference, we used a list of all proteins present in
903 the deep fractionated DDA spectral library. The complete list of differentially regulated pathways,
904 corresponding proteins, reference pathway annotations, statistics, and source databases are
905 available as a supplemental file (Table S4j, k). To generate dot plot representations of pathway
906 analysis, we used the "ggplot2" package in R.

907 **Author Contributions**

908 Conceptualization, BS, JC, ESB; experiments and methodology, SKP, JB, JRC, JPR, RLB, RB,
909 LR; data processing, SKP, JB, JRC, RLB, LR; writing original draft, SKP, PYD, JRC; Figures, SKP,
910 JRC, JB, BS; review and editing of the manuscript, BS, JB, JRC, ESB, MAW, CW, JBB, JC, LR.

911

912 **Conflicts of interest**

913 Dr. Judith Campisi was a co-founder and a shareholder of Unity Biotechnology. Drs. Roland
914 Bruderer and Lukas Reiter are employees of Biognosys AG. Spectronaut and the iRT kit are
915 trademarks of Biognosys AG. The other authors declare no conflicts of interest.

916

917 **Acknowledgments**

918 This work is supported by grants from the National Institutes of Health under award numbers U01
919 AG060906 (Schilling), U01 AG060906-02S1 and NCRR shared instrumentation grant S10
920 OD028654 (Schilling), U54 AG075932 (Schilling, Melov), P01 AG066591 (Ellerby), P01 AG017242
921 (Campisi) and R01 AG051729 (Campisi), P42 ES027704 (Baker), R01 GM141277 (Baker) and
922 RM1 GM145416 (Baker). Dr. Patel was supported by a Glenn Fellowship in Aging Research from
923 the Glenn Foundation. We thank John Carroll for providing graphical support and LC Sciences for
924 miRNA Sequencing Services. Dr. Schilling and team were deeply saddened about the passing of
925 Dr. Campisi and would like to recognize her as amazing scientist, mentor and friend.

926

927

928 **Figure Legends**

929 **Fig. 1: Multi-omics workflow for aging/senescence exosome biomarker discovery.**

930 **A.** Two different sample types, primary human lung fibroblasts and human plasma, were
931 investigated. Three senescence stimuli, Irradiation; IR, Doxorubicin; doxo, and Antimycin A-
932 induced mitochondrial dysfunction-associated senescence; MiDAS, were used to generate
933 senescent primary human lung fibroblasts (n=4, each condition). Quiescent cells (Qui) or DMSO-
934 treated fibroblasts were used as control. Plasma from young (20-26 years old) and older (65-74
935 years old) individuals was used (n=5 each). Exosomes were enriched by sequential size-
936 exclusion chromatography and ultrafiltration (SEC/UF). Immunoblotting and particle size

937 analysis was conducted to confirm enriched, high-quality, and intact exosomes. Three different
938 protein spectral libraries; DDA, directDIA, and hybrid, were generated. Multicomponent
939 Senescence/Aging Biomarkers were identified by high-throughput quantitative exosome multi-
940 omics (proteomics, lipidomics, and miRNA) analysis.

941

942 **Fig. 2: Exosome enrichment from plasma and primary human lung fibroblasts (IMR90)**
943 **and characterization.**

944 **A.** Exosome isolation workflow using sequential size-exclusion chromatography and
945 ultrafiltration (SEC/UF). **B.** Scheme for SEC fraction collection. **C.** Spectrophotometric
946 quantification of exosomes in SEC fractions. Red, Exosome (OD_{600}); Blue, plasma proteins
947 (OD_{280}, dilution 1:20). **D.** Exosome size distribution analysis by qNano Gold. Mean diameter;
948 135 nm, Mode diameter; 107 nm. **E.** Immunoblot of exosome protein markers; CD9 antigen
949 (CD9) and Tumor susceptibility gene 101 protein (TSG101) in different exosome fractions to
950 confirm enrichment. IgG and albumin were used as determinants of plasma protein
951 contaminants. E1–E5: exosome fractions, P1: the pool of fractions 11 + 12, and P10: the pool
952 of fractions 29 + 30 (1:20 dilution) were loaded for comparison between plasma proteins and
953 exosome fractions. **F.** Semi-quantitative estimation of the volume intensities of western blot
954 bands using Image J software.

955

956 **Fig. 3: Senescence stimuli specific exosome protein signatures in primary human lung**
957 **fibroblasts (IMR90).**

958 **A (i).** Study design showing three different senescence stimuli, Irradiation; IR, Doxorubicin; doxo,
959 and Antimycin A-induced mitochondrial dysfunction-associated senescence; MiDAS, were used
960 to generate senescent primary human lung fibroblasts (n=4, each condition), and Quiescent cells
961 (Qui) were used as control. **(ii)** A timeline indicating treatment days and endpoints for the three
962 different senescence inducers and control conditions. **B.** Bar graph showing the percentage of
963 viable and senescent fibroblasts in the different senescence-induction conditions using Edu
964 (shown in blue) and SA-β-Gal (shown in red). **C.** Summary of significantly altered exosome
965 proteins (q-value < 0.05 and ≥ 1.5-fold change) in senescent human lung fibroblasts compared

966 to quiescent cells following IR, doxo, and MiDAS senescence induction. **D.** Venn diagram
967 showing overlapping and unique protein signatures of senescent human lung fibroblast
968 exosomes induced by IR, doxo, and MiDAS. **E.** Heatmap displaying the exosome protein fold
969 change averaged across replicates, showing the top 18 altered proteins, increased (red) and
970 decreased (blue) due to senescence. The intensities averaged for Qui were used as the
971 baseline. ClueGO biological pathways and cell compartments are presented. BP; Biological
972 process, CC; Cellular process. **F.** Partial least squares-discriminant analysis (PLS-DA) clustered
973 senescent fibroblasts from Quiescent control. The two variates explaining the most significant
974 variations are shown. **G.** Venn diagram showing overlapping and unique exosome SASP (sEVs)
975 and soluble SASP protein signatures of IR-induced senescent fibroblasts. **H.** Enrichment
976 analysis of Gene Ontology/cellular compartments overrepresented among protein contents of
977 senescent fibroblast exosomes. **I.** Venn diagram showing overlapping and unique surface
978 protein signatures of senescent fibroblast exosomes induced by IR, doxo, and MiDAS. **J.** Bar
979 graph showing malondialdehyde cellular content, a product of lipid peroxidation used as a
980 marker for intracellular oxidative stress measured in the different senescence stimuli.

981

982 **Fig. 4: Age-specific plasma exosome protein signatures in old and young cohorts.**

983 **A.** Partial least squares-discriminant analysis (PLS-DA) clustered old and young cohorts based
984 on 1356 protein groups. The two variates explaining the most significant variations are shown.
985 **B.** Volcano plot showing significantly altered age-specific plasma exosome proteins (q-value <
986 0.05 and ≥ 1.5-fold). Red, upregulated; Blue, downregulated; and Gray, No significant change.
987 A few selected differentially abundant proteins are labeled. **C.** Heatmap displaying the plasma
988 exosome protein fold change averaged across replicates, showing the top 26 altered proteins
989 increased (red) and decreased (blue) due to Aging. The intensities averaged for young plasma
990 exosomes were used as the baseline. ClueGO biological pathways and cell compartments are
991 presented. BP; Biological process, CC; Cellular process. P-value * ≤ 0.05, ** ≤ 0.01, *** ≤ 0.001.
992 **D.** The most significant age-related exosome protein pathways are (i) upregulated and (ii)
993 downregulated. **E.** Enrichment analysis of gene-ontology/cellular compartments
994 overrepresented among aging exosome proteins. **F.** Three examples of individual protein MS
995 intensities and how the intensity changes with age**.**

996 **Fig. 5: Senescence stimuli specific exosome lipid signatures in primary human lung**
997 **fibroblasts (IMR90).**

998 **A.** Summary of significantly altered exosome lipids (p-value < 0.05 and > 2-fold change) from
999 senescent human lung fibroblasts compared to quiescent cells following IR, doxo, and MiDAS
1000 senescence induction. **B.** Partial least squares-discriminant analysis (PLS-DA) clustered
1001 senescent human lung fibroblasts from Quiescent (control) based on 247 lipids **(i)** Low serum
1002 media (LSM; Qui IR-mock control) vs IR **(ii)** Low serum media (Qui DMSO control) vs doxo and
1003 MiDAS. **C.** Heatmap of 145 differentially expressed exosome lipids from 15 different classes.
1004 Clustering was performed using Euclidean distance and complete linkage and $\log_2$ fold change
1005 is illustrated to visualize trends with the three senescence inducers. **D.** Violin plots showing three
1006 examples of individual lipid profiles where PC(18:0/20:4) and SM(d18:2/16:0) were upregulated
1007 with all senescence inducers, while TB(54:6) was downregulated in IR and doxo but not MiDAS,
1008 illustrating lipid response differences due to different stimuli. AC: Acylcarnitine, Cer: Ceramide,
1009 FA: Fatty acid, HexCer: Hexosylceramide, LPC: Lysophosphatidylcholine, PA: Phosphatidic
1010 acid, PC: Phosphatidylcholine, PE: Phosphatidylethanolamine, PG: Phosphatidylglycerol, PI:
1011 Phosphatidylinositol, PS: Phosphatidylserine, SM: Sphingomyelin, TG: Triglycerides.

1012

1013 **Fig. 6. Overview of top potential exosome biomarkers for senescence and aging.**
1014 **A.** Exosome proteins and miRNAs identified as potential biomarkers for secondary senescence
1015 (paracrine) and aging. **B.** Venn diagram showing overlapping and unique exosome proteins in
1016 senescent primary human lung fibroblasts (IMR90) and plasma from aging cohorts. Heatmap
1017 showing the top 15 commonly altered proteins in senescent fibroblasts and plasma from aging
1018 cohorts.

1019

1020 **Fig. 7. Summary of exosome-mediated intercellular communication in senescence and**
1021 **aging.**
1022 A summary of our overall exosome proteomic findings from senescent human primary lung
1023 fibroblast cells that suggest potential mechanisms by which senescence is exacerbated and
1024 propagated to cause secondary senescence. Changes in inflammatory, antioxidants, and matrix
1025 remodeling-related proteins in exosomes (eSASP) from senescent cells may contribute to

1026 creating a senescent microenvironment that may influence and affect neighboring cells.
1027 Heatmaps show the top selected senescent fibroblast exosome proteins involved in
1028 inflammation, antioxidant, and ECM-remodeling pathways.

1029 **References:**

1030

1031 1. Organization TWH. Ageing and health: WHO; 2022 [2023]. Available from:
1032 https://www.who.int/news-room/fact-sheets/detail/ageing-and-health
1033 2. Kennedy BK, Berger SL, Brunet A, Campisi J, Cuervo AM, Epel ES, et al. Geroscience:
1034 linking aging to chronic disease. Cell. 2014;159(4):709-13. doi: 10.1016/j.cell.2014.10.039.
1035 PubMed PMID: 25417146; PubMed Central PMCID: PMCPMC4852871.
1036 3. Scott AJ, Ellison M, Sinclair DA. The economic value of targeting aging. Nature Aging.
1037 2021;1(7):616-23. doi: 10.1038/s43587-021-00080-0.
1038 4. López-Otín C, Blasco MA, Partridge L, Serrano M, Kroemer G. The hallmarks of aging. Cell.
1039 2013;153(6):1194-217. doi: 10.1016/j.cell.2013.05.039.
1040 5. Bodnar AG, Ouellette M, Frolkis M, Holt SE, Chiu CP, Morin GB, et al. Extension of life-span
1041 by introduction of telomerase into normal human cells. Science. 1998;279(5349):349-52.
1042 Epub 1998/02/07. doi: 10.1126/science.279.5349.349. PubMed PMID: 9454332.
1043 6. Wiley CD, Velarde MC, Lecot P, Liu S, Sarnoski EA, Freund A, et al. Mitochondrial
1044 Dysfunction Induces Senescence with a Distinct Secretory Phenotype. Cell Metab.
1045 2016;23(2):303-14. Epub 20151210. doi: 10.1016/j.cmet.2015.11.011. PubMed PMID:
1046 26686024; PubMed Central PMCID: PMCPMC4749409.
1047 7. van Deursen JM. The role of senescent cells in ageing. Nature. 2014;509(7501):439-46.
1048 Epub 2014/05/23. doi: 10.1038/nature13193. PubMed PMID: 24848057; PubMed Central
1049 PMCID: PMCPMC4214092.
1050 8. Sax K. Chromosome Aberrations Induced by X-Rays. Genetics. 1938;23(5):494-516. doi:
1051 10.1093/genetics/23.5.494. PubMed PMID: 17246897; PubMed Central PMCID:
1052 PMCPMC1209022.
1053 9. Goto S, Ihara Y, Urata Y, Izumi S, Abe K, Koji T, et al. Doxorubicin-induced DNA intercalation
1054 and scavenging by nuclear glutathione S-transferase pi. FASEB J. 2001;15(14):2702-14. doi:
1055 10.1096/fj.01-0376com. PubMed PMID: 11726546.
1056 10. Basisty N, Kale A, Jeon OH, Kuehnemann C, Payne T, Rao C, et al. A proteomic atlas of
1057 senescence-associated secretomes for aging biomarker development. PLoS Biology.
1058 2020;18(1):e3000599-e. doi: 10.1371/journal.pbio.3000599.

1059 11. Coppé JP, Patil CK, Rodier F, Sun Y, Muñoz DP, Goldstein J, et al. Senescence-associated
1060 secretory phenotypes reveal cell-nonautonomous functions of oncogenic RAS and the p53
1061 tumor suppressor. PLoS biology. 2008;6(12). doi: 10.1371/journal.pbio.0060301.
1062 12. Coppe JP, Patil CK, Rodier F, Krtolica A, Beausejour CM, Parrinello S, et al. A human-like
1063 senescence-associated secretory phenotype is conserved in mouse cells dependent on
1064 physiological oxygen. PLoS One. 2010;5(2):e9188. Epub 2010/02/20. doi:
1065 10.1371/journal.pone.0009188. PubMed PMID: 20169192; PubMed Central PMCID:
1066 PMCPMC2820538.
1067 13. Borghesan M, Fafián-Labora J, Eleftheriadou O, Carpintero-Fernández P, Paez-Ribes M,
1068 Vizcay-Barrena G, et al. Small Extracellular Vesicles Are Key Regulators of Non-cell
1069 Autonomous Intercellular Communication in Senescence via the Interferon Protein IFITM3.
1070 Cell Reports. 2019;27(13):3956-71.e6. doi: 10.1016/j.celrep.2019.05.095.
1071 14. Gorgoulis V, Adams PD, Alimonti A, Bennett DC, Bischof O, Bishop C, et al. Cellular
1072 Senescence: Defining a Path Forward. Cell. 2019;179(4):813-27. doi:
1073 10.1016/j.cell.2019.10.005.
1074 15. Wiley CD, Sharma R, Davis SS, Lopez-Dominguez JA, Mitchell KP, Wiley S, et al. Oxylipin
1075 biosynthesis reinforces cellular senescence and allows detection of senolysis. Cell Metab.
1076 2021;33(6):1124-36 e5. Epub 2021/04/04. doi: 10.1016/j.cmet.2021.03.008. PubMed PMID:
1077 33811820; PubMed Central PMCID: PMCPMC8501892.
1078 16. Elliott RO, He M. Unlocking the Power of Exosomes for Crossing Biological Barriers in Drug
1079 Delivery. Pharmaceutics. 2021;13(1). Epub 20210119. doi:
1080 10.3390/pharmaceutics13010122. PubMed PMID: 33477972; PubMed Central PMCID:
1081 PMCPMC7835896.
1082 17. D'Anca M, Fenoglio C, Serpente M, Arosio B, Cesari M, Scarpini EA, et al. Exosome
1083 Determinants of Physiological Aging and Age-Related Neurodegenerative Diseases. Front
1084 Aging Neurosci. 2019;11:232. Epub 20190828. doi: 10.3389/fnagi.2019.00232. PubMed
1085 PMID: 31555123; PubMed Central PMCID: PMCPMC6722391.
1086 18. Abramowicz A, Widlak P, Pietrowska M. Proteomic analysis of exosomal cargo: The
1087 challenge of high purity vesicle isolation. Molecular BioSystems. 2016;12(5):1407-19. doi:
1088 10.1039/c6mb00082g.

1089 19. Greening DW, Xu R, Ji H, Tauro BJ, Simpson RJ. A protocol for exosome isolation and
1090 characterization: evaluation of ultracentrifugation, density-gradient separation, and
1091 immunoaffinity capture methods. Methods Mol Biol. 2015;1295:179-209. doi: 10.1007/978-
1092 1-4939-2550-6_15. PubMed PMID: 25820723.
1093 20. Wu CC, Tsantilas KA, Park J, Plubell D, Sanders JA, Naicker P, et al. Mag-Net: Rapid
1094 enrichment of membrane-bound particles enables high coverage quantitative analysis of the
1095 plasma proteome. bioRxiv. 2024. Epub 2024/04/15. doi: 10.1101/2023.06.10.544439.
1096 PubMed PMID: 38617345; PubMed Central PMCID: PMCPMC11014469
1097 21. Cvjetkovic A, Lotvall J, Lasser C. The influence of rotor type and centrifugation time on the
1098 yield and purity of extracellular vesicles. J Extracell Vesicles. 2014;3. Epub 20140325. doi:
1099 10.3402/jev.v3.23111. PubMed PMID: 24678386; PubMed Central PMCID:
1100 PMCPMC3967015.
1101 22. Boing AN, van der Pol E, Grootemaat AE, Coumans FA, Sturk A, Nieuwland R. Single-step
1102 isolation of extracellular vesicles by size-exclusion chromatography. J Extracell Vesicles.
1103 2014;3. Epub 20140908. doi: 10.3402/jev.v3.23430. PubMed PMID: 25279113; PubMed
1104 Central PMCID: PMCPMC4159761.
1105 23. Collins BC, Hunter CL, Liu Y, Schilling B, Rosenberger G, Bader SL, et al. Multi-laboratory
1106 assessment of reproducibility, qualitative and quantitative performance of SWATH-mass
1107 spectrometry. Nat Commun. 2017;8(1):291. Epub 20170821. doi: 10.1038/s41467-017-
1108 00249-5. PubMed PMID: 28827567; PubMed Central PMCID: PMCPMC5566333.
1109 24. Schilling B, Gibson BW, Hunter CL. Generation of High-Quality SWATH((R)) Acquisition Data
1110 for Label-free Quantitative Proteomics Studies Using TripleTOF((R)) Mass Spectrometers.
1111 Methods Mol Biol. 2017;1550:223-33. doi: 10.1007/978-1-4939-6747-6_16. PubMed PMID:
1112 28188533; PubMed Central PMCID: PMCPMC5669615.
1113 25. Gillet LC, Navarro P, Tate S, Rost H, Selevsek N, Reiter L, et al. Targeted data extraction of
1114 the MS/MS spectra generated by data-independent acquisition: a new concept for consistent
1115 and accurate proteome analysis. Mol Cell Proteomics. 2012;11(6):O111 016717. Epub
1116 2012/01/21. doi: 10.1074/mcp.O111.016717. PubMed PMID: 22261725; PubMed Central
1117 PMCID: PMCPMC3433915.
1118 26. Guan S, Yu H, Yan G, Gao M, Sun W, Zhang X. Characterization of Urinary Exosomes
1119 Purified with Size Exclusion Chromatography and Ultracentrifugation. J Proteome Res.

1120 2020;19(6):2217-25. Epub 20200428. doi: 10.1021/acs.jproteome.9b00693. PubMed PMID:
1121 32248692.
1122 27. Keerthikumar S, Chisanga D, Ariyaratne D, Al Saffar H, Anand S, Zhao K, et al. ExoCarta: A
1123 Web-Based Compendium of Exosomal Cargo. J Mol Biol. 2016;428(4):688-92. Epub
1124 20151003. doi: 10.1016/j.jmb.2015.09.019. PubMed PMID: 26434508; PubMed Central
1125 PMCID: PMCPMC4783248.
1126 28. Evans DS, Young D, Tanaka T, Basisty N, Bandinelli S, Ferrucci L, et al. Proteomic Analysis
1127 of the Senescence-Associated Secretory Phenotype: GDF-15, IGFBP-2, and Cystatin-C Are
1128 Associated With Multiple Aging Traits. J Gerontol A Biol Sci Med Sci. 2024;79(3). Epub
1129 2023/11/20. doi: 10.1093/gerona/glad265. PubMed PMID: 37982669; PubMed Central
1130 PMCID: PMCPMC10876076.
1131 29. Tanaka T, Basisty N, Fantoni G, Candia J, Moore AZ, Biancotto A, et al. Plasma proteomic
1132 biomarker signature of age predicts health and life span. Elife. 2020;9. Epub 2020/11/20. doi:
1133 10.7554/eLife.61073. PubMed PMID: 33210602; PubMed Central PMCID:
1134 PMCPMC7723412.
1135 30. Venable ME, Lee JY, Smyth MJ, Bielawska A, Obeid LM. Role of ceramide in cellular
1136 senescence. J Biol Chem. 1995;270(51):30701-8. doi: 10.1074/jbc.270.51.30701. PubMed
1137 PMID: 8530509.
1138 31. Bitencourt TC, Vargas JE, Silva AO, Fraga LR, Filippi-Chiela E. Subcellular structure,
1139 heterogeneity, and plasticity of senescent cells. Aging Cell. 2024;23(4):e14154. Epub
1140 2024/03/30. doi: 10.1111/acel.14154. PubMed PMID: 38553952; PubMed Central PMCID:
1141 PMCPMC11019148.
1142 32. Johnson AA, Shokhirev MN, Wyss-Coray T, Lehallier B. Systematic review and analysis of
1143 human proteomics aging studies unveils a novel proteomic aging clock and identifies key
1144 processes that change with age. Ageing Res Rev. 2020;60:101070. Epub 2020/04/21. doi:
1145 10.1016/j.arr.2020.101070. PubMed PMID: 32311500.
1146 33. Panigrahi GK, Praharaj PP, Kittaka H, Mridha AR, Black OM, Singh R, et al. Exosome
1147 proteomic analyses identify inflammatory phenotype and novel biomarkers in African
1148 American prostate cancer patients. Cancer Med. 2019;8(3):1110-23. Epub 20190108. doi:
1149 10.1002/cam4.1885. PubMed PMID: 30623593; PubMed Central PMCID:
1150 PMCPMC6434210.

1151 34. Khansari N, Shakiba Y, Mahmoudi M. Chronic inflammation and oxidative stress as a major
1152 cause of age-related diseases and cancer. Recent Pat Inflamm Allergy Drug Discov.
1153 2009;3(1):73-80. doi: 10.2174/187221309787158371. PubMed PMID: 19149749.
1154 35. Sorokin L. The impact of the extracellular matrix on inflammation. Nat Rev Immunol.
1155 2010;10(10):712-23. doi: 10.1038/nri2852. PubMed PMID: 20865019.
1156 36. Levi N, Papismadov N, Solomonov I, Sagi I, Krizhanovsky V. The ECM path of senescence
1157 in aging: components and modifiers. FEBS J. 2020;287(13):2636-46. Epub 20200320. doi:
1158 10.1111/febs.15282. PubMed PMID: 32145148.
1159 37. Blokland KEC, Pouwels SD, Schuliga M, Knight DA, Burgess JK. Regulation of cellular
1160 senescence by extracellular matrix during chronic fibrotic diseases. Clin Sci (Lond).
1161 2020;134(20):2681-706. doi: 10.1042/CS20190893. PubMed PMID: 33084883; PubMed
1162 Central PMCID: PMCPMC7578566.
1163 38. Lamontagne-Proulx J, St-Amour I, Labib R, Pilon J, Denis HL, Cloutier N, et al. Portrait of
1164 blood-derived extracellular vesicles in patients with Parkinson's disease. Neurobiol Dis.
1165 2019;124:163-75. Epub 20181105. doi: 10.1016/j.nbd.2018.11.002. PubMed PMID:
1166 30408591.
1167 39. Urbanelli L, Buratta S, Sagini K, Tancini B, Emiliani C. Extracellular Vesicles as New Players
1168 in Cellular Senescence. Int J Mol Sci. 2016;17(9). Epub 20160826. doi:
1169 10.3390/ijms17091408. PubMed PMID: 27571072; PubMed Central PMCID:
1170 PMCPMC5037688.
1171 40. Borghesan M, O'Loghlen A. Integrins in senescence and aging. Cell Cycle. 2017;16(10):909-
1172 10. Epub 20170501. doi: 10.1080/15384101.2017.1316573. PubMed PMID: 28459356;
1173 PubMed Central PMCID: PMCPMC5462089.
1174 41. Elzi DJ, Lai Y, Song M, Hakala K, Weintraub ST, Shiio Y. Plasminogen activator inhibitor 1-
1175 -insulin-like growth factor binding protein 3 cascade regulates stress-induced senescence.
1176 Proc Natl Acad Sci U S A. 2012;109(30):12052-7. Epub 20120709. doi:
1177 10.1073/pnas.1120437109. PubMed PMID: 22778398; PubMed Central PMCID:
1178 PMCPMC3409757.
1179 42. Kortlever RM, Higgins PJ, Bernards R. Plasminogen activator inhibitor-1 is a critical
1180 downstream target of p53 in the induction of replicative senescence. Nat Cell Biol.

1181 2006;8(8):877-84. Epub 20060723. doi: 10.1038/ncb1448. PubMed PMID: 16862142;
1182 PubMed Central PMCID: PMCPMC2954492.
1183 43. Benatar T, Yang W, Amemiya Y, Evdokimova V, Kahn H, Holloway C, et al. IGFBP7 reduces
1184 breast tumor growth by induction of senescence and apoptosis pathways. Breast Cancer
1185 Res Treat. 2012;133(2):563-73. Epub 20111014. doi: 10.1007/s10549-011-1816-4. PubMed
1186 PMID: 21997538.
1187 44. Severino V, Alessio N, Farina A, Sandomenico A, Cipollaro M, Peluso G, et al. Insulin-like
1188 growth factor binding proteins 4 and 7 released by senescent cells promote premature
1189 senescence in mesenchymal stem cells. Cell Death Dis. 2013;4(11):e911. Epub 20131107.
1190 doi: 10.1038/cddis.2013.445. PubMed PMID: 24201810; PubMed Central PMCID:
1191 PMCPMC3847322.
1192 45. Senturk S, Mumcuoglu M, Gursoy-Yuzugullu O, Cingoz B, Akcali KC, Ozturk M.
1193 Transforming growth factor-beta induces senescence in hepatocellular carcinoma cells and
1194 inhibits tumor growth. Hepatology. 2010;52(3):966-74. doi: 10.1002/hep.23769. PubMed
1195 PMID: 20583212.
1196 46. Tasaki M, Ueda M, Ochiai S, Tanabe Y, Murata S, Misumi Y, et al. Transmission of circulating
1197 cell-free AA amyloid oligomers in exosomes vectors via a prion-like mechanism. Biochem
1198 Biophys Res Commun. 2010;400(4):559-62. doi: 10.1016/J.BBRC.2010.08.101.
1199 47. Jiang R, Rong C, Ke R, Meng S, Yan X, Ke H, et al. Differential proteomic analysis of serum
1200 exosomes reveals alterations in progression of Parkinson disease. Medicine (Baltimore).
1201 2019;98(41):e17478. doi: 10.1097/MD.0000000000017478.
1202 48. Hamsanathan S, Gurkar AU. Lipids as Regulators of Cellular Senescence. Front Physiol.
1203 2022;13:796850. Epub 20220304. doi: 10.3389/fphys.2022.796850. PubMed PMID:
1204 35370799; PubMed Central PMCID: PMCPMC8965560.
1205 49. Flor AC, Wolfgeher D, Wu D, Kron SJ. A signature of enhanced lipid metabolism, lipid
1206 peroxidation and aldehyde stress in therapy-induced senescence. Cell Death Discov.
1207 2017;3:17075. Epub 20171030. doi: 10.1038/cddiscovery.2017.75. PubMed PMID:
1208 29090099; PubMed Central PMCID: PMCPMC5661608.
1209 50. Wu D, Yan J, Shen X, Sun Y, Thulin M, Cai Y, et al. Profiling surface proteins on individual
1210 exosomes using a proximity barcoding assay. Nat Commun. 2019;10(1):3854. doi:
1211 10.1038/S41467-019-11486-1.

1212 51. Serpente M, Fenoglio C, D'Anca M, Arcaro M, Sorrentino F, Visconte C, et al. MiRNA Profiling
1213 in Plasma Neural-Derived Small Extracellular Vesicles from Patients with Alzheimer's
1214 Disease. Cells. 2020;9(6). Epub 20200610. doi: 10.3390/cells9061443. PubMed PMID:
1215 32531989; PubMed Central PMCID: PMCPMC7349735.
1216 52. Sheinerman KS, Tsivinsky VG, Abdullah L, Crawford F, Umansky SR. Plasma microRNA
1217 biomarkers for detection of mild cognitive impairment: biomarker validation study. Aging
1218 (Albany NY). 2013;5(12):925-38. doi: 10.18632/aging.100624. PubMed PMID: 24368295;
1219 PubMed Central PMCID: PMCPMC3883708.
1220 53. Sheinerman KS, Toledo JB, Tsivinsky VG, Irwin D, Grossman M, Weintraub D, et al.
1221 Circulating brain-enriched microRNAs as novel biomarkers for detection and differentiation
1222 of neurodegenerative diseases. Alzheimers Res Ther. 2017;9(1):89. Epub 20171109. doi:
1223 10.1186/s13195-017-0316-0. PubMed PMID: 29121998; PubMed Central PMCID:
1224 PMCPMC5679501.
1225 54. Bruderer R, Bernhardt OM, Gandhi T, Xuan Y, Sondermann J, Schmidt M, et al. Optimization
1226 of Experimental Parameters in Data-Independent Mass Spectrometry Significantly Increases
1227 Depth and Reproducibility of Results. Mol Cell Proteomics. 2017;16(12):2296-309. Epub
1228 20171025. doi: 10.1074/mcp.RA117.000314. PubMed PMID: 29070702; PubMed Central
1229 PMCID: PMCPMC5724188.
1230 55. Muntel J, Gandhi T, Verbeke L, Bernhardt OM, Treiber T, Bruderer R, et al. Surpassing 10
1231 000 identified and quantified proteins in a single run by optimizing current LC-MS
1232 instrumentation and data analysis strategy. Mol Omics. 2019;15(5):348-60. doi:
1233 10.1039/c9mo00082h. PubMed PMID: 31465043.
1234 56. Reiter L, Claassen M, Schrimpf SP, Jovanovic M, Schmidt A, Buhmann JM, et al. Protein
1235 identification false discovery rates for very large proteomics data sets generated by tandem
1236 mass spectrometry. Mol Cell Proteomics. 2009;8(11):2405-17. Epub 20090716. doi:
1237 10.1074/mcp.M900317-MCP200. PubMed PMID: 19608599; PubMed Central PMCID:
1238 PMCPMC2773710.
1239 57. Folch J, Lees M, Sloane Stanley GH. A simple method for the isolation and purification of
1240 total lipides from animal tissues. J Biol Chem. 1957;226(1):497-509. PubMed PMID:
1241 13428781.

1242 58. Ulmer CZ, Jones CM, Yost RA, Garrett TJ, Bowden JA. Optimization of Folch, Bligh-Dyer,
1243 and Matyash sample-to-extraction solvent ratios for human plasma-based lipidomics studies.
1244 Anal Chim Acta. 2018;1037:351-7. Epub 20180808. doi: 10.1016/j.aca.2018.08.004.
1245 PubMed PMID: 30292311; PubMed Central PMCID: PMCPMC6261534.
1246 59. Stow SM, Causon TJ, Zheng X, Kurulugama RT, Mairinger T, May JC, et al. An
1247 Interlaboratory Evaluation of Drift Tube Ion Mobility-Mass Spectrometry Collision Cross
1248 Section Measurements. Anal Chem. 2017;89(17):9048-55. Epub 20170816. doi:
1249 10.1021/acs.analchem.7b01729. PubMed PMID: 28763190; PubMed Central PMCID:
1250 PMCPMC5744684.
1251 60. Gao X, Zhang Q, Meng D, Isaac G, Zhao R, Fillmore TL, et al. A reversed-phase capillary
1252 ultra-performance liquid chromatography-mass spectrometry (UPLC-MS) method for
1253 comprehensive top-down/bottom-up lipid profiling. Anal Bioanal Chem. 2012;402(9):2923-
1254 33. Epub 20120223. doi: 10.1007/s00216-012-5773-5. PubMed PMID: 22354571; PubMed
1255 Central PMCID: PMCPMC3531553.
1256 61. Baker ES, Tang K, Danielson WF, 3rd, Prior DC, Smith RD. Simultaneous fragmentation of
1257 multiple ions using IMS drift time dependent collision energies. J Am Soc Mass Spectrom.
1258 2008;19(3):411-9. Epub 20071204. doi: 10.1016/j.jasms.2007.11.018. PubMed PMID:
1259 18226544; PubMed Central PMCID: PMCPMC2517259.
1260 62. Kirkwood KI, Christopher MW, Burgess JL, Littau SR, Foster K, Richey K, et al. Development
1261 and Application of Multidimensional Lipid Libraries to Investigate Lipidomic Dysregulation
1262 Related to Smoke Inhalation Injury Severity. J Proteome Res. 2022;21(1):232-42. Epub
1263 20211207. doi: 10.1021/acs.jproteome.1c00820. PubMed PMID: 34874736; PubMed
1264 Central PMCID: PMCPMC8741653.
1265 63. Li M, Xia Y, Gu Y, Zhang K, Lang Q, Chen L, et al. MicroRNAome of porcine pre- and
1266 postnatal development. PLoS One. 2010;5(7):e11541. Epub 20100712. doi:
1267 10.1371/journal.pone.0011541. PubMed PMID: 20634961; PubMed Central PMCID:
1268 PMCPMC2902522.

1269

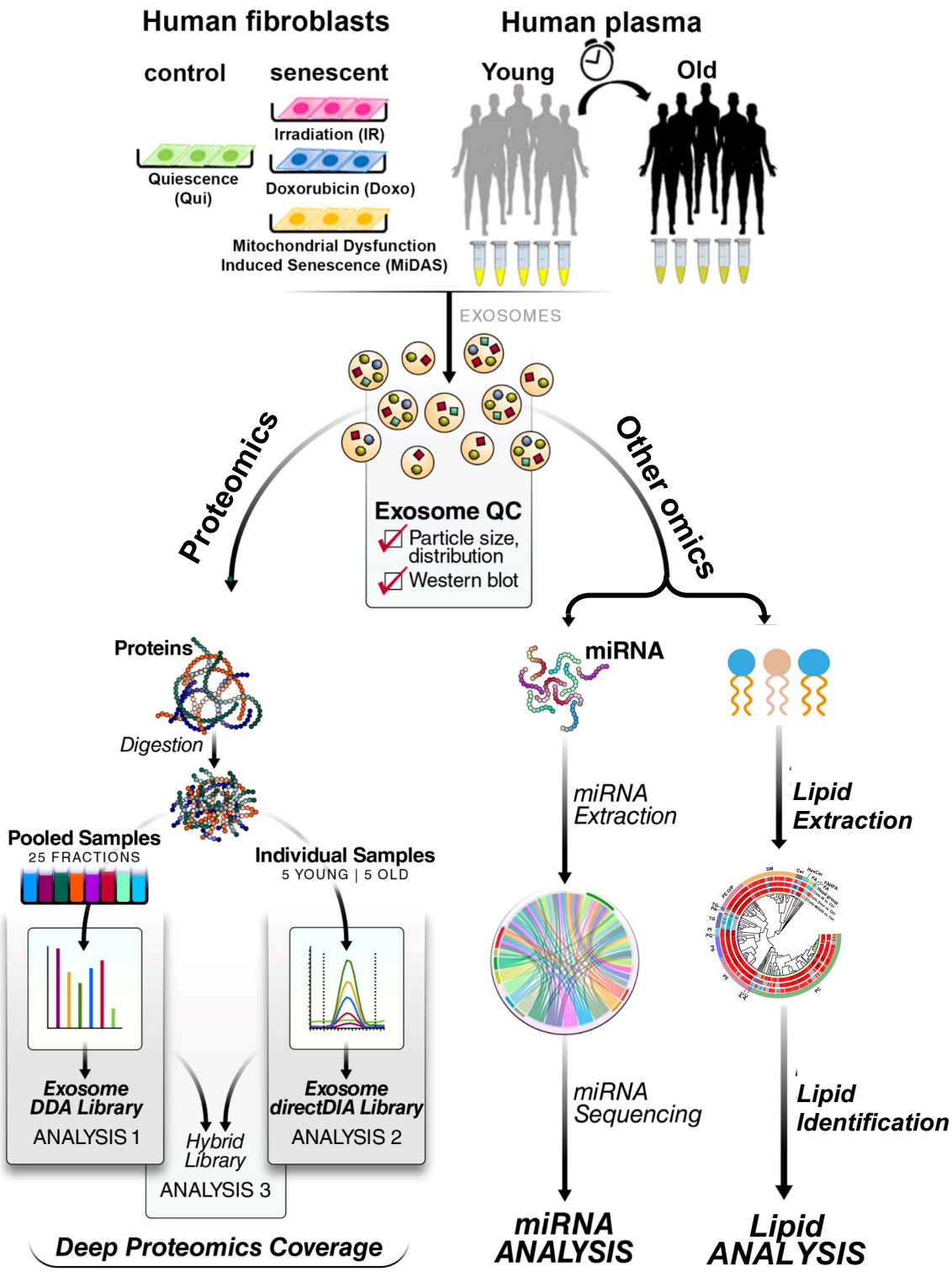
Human fibroblasts
control
senescent
Quiescence (Qui)
Irradiation (IR)
Doxorubicin (Doxo)
Mitochondrial Dysfunction Induced Senescence (MiDAS)
Human plasma
Young
Old
EXOSOMES
Proteomics
Other omics
Exosome QC
Particle size, distribution
Western blot
Proteins
Digestion
Pooled Samples
25 FRACTIONS
Individual Samples
5 YOUNG | 5 OLD
Exosome DDA Library
ANALYSIS 1
Hybrid Library
ANALYSIS 3
Exosome directDIA Library
ANALYSIS 2
Deep Proteomics Coverage
miRNA
miRNA Extraction
miRNA Sequencing
miRNA ANALYSIS
Lipid Extraction
Lipid Identification
Lipid ANALYSIS

Fig. 1

A. SEC/UF is ideal for exosome proteomics analysis

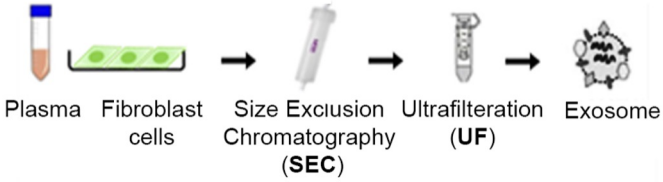

B. SEC fractionation scheme

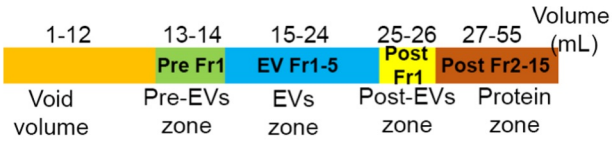

C. Exosome tracking in SEC fractions by UV-vis spectrophotometer

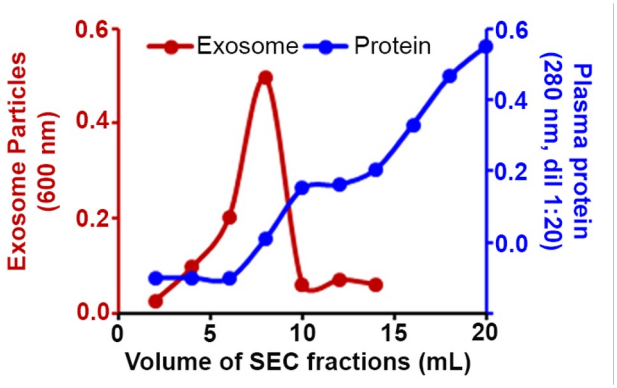

D. Size distribution histogram confirms intact exosome

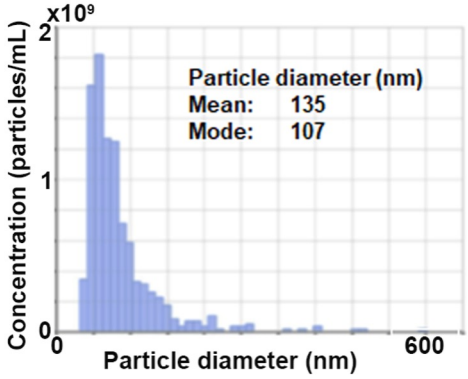

E. Western blot confirms enrichment of exosomes

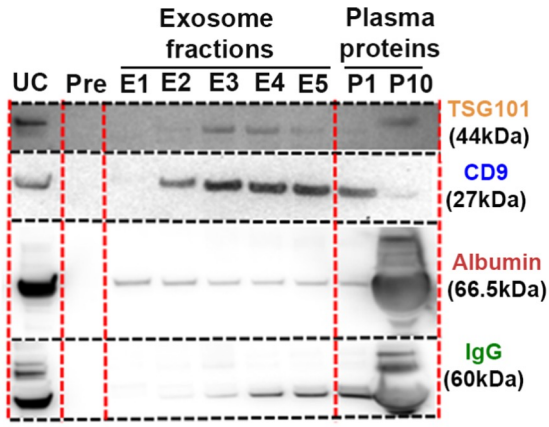

F. Semi-quantitative estimation of western blot bands

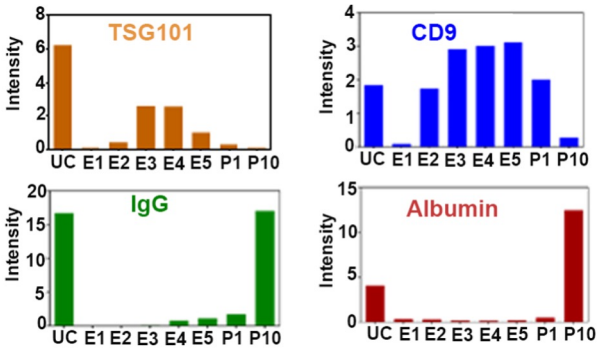

Fig. 2

A. Study design for senescence induction in fibroblasts by three different stressors

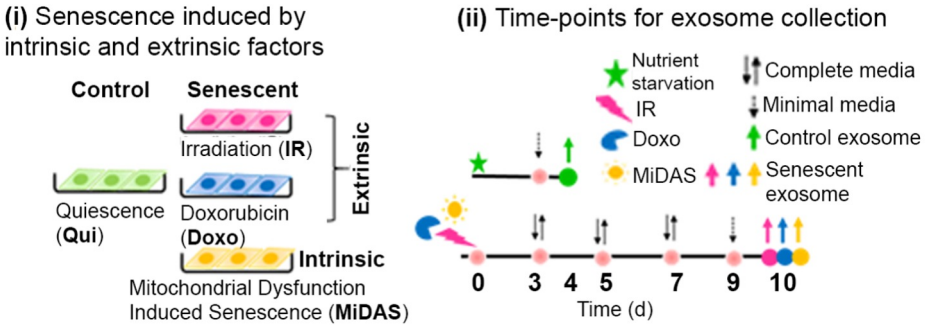

B. Determination of senescent and viable fibroblasts

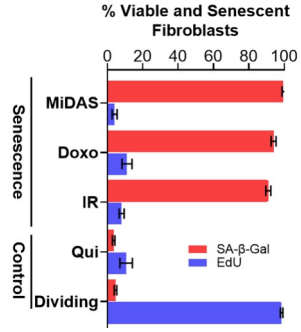

C. Senescent fibroblast exosome protein profile

Induction	# Proteins identified	# Proteins altered
IR extrinsic	1426	742 ↑ 120 ↓
DOXO extrinsic	1426	295 ↑ 387 ↓
MiDAS intrinsic	1426	66 ↑ 1078 ↓

D. Common and unique exosome proteins in senescent fibroblasts

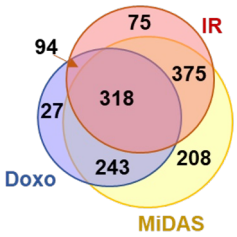

E. Heatmap: Common exosome proteins in all senescence stimuli

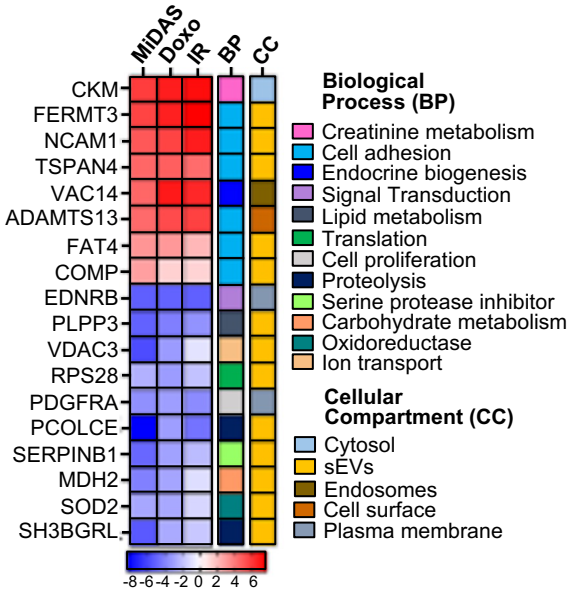

F. Supervised clustering classifies senescent fibroblast exosomes

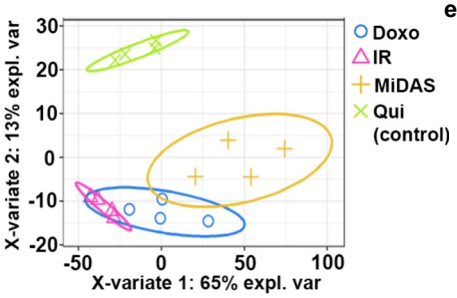

G. Common and unique proteins in IR SASP and exosomes

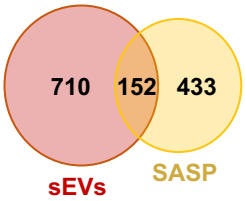

H. *In silico* prediction of senescent exosome cell compartments

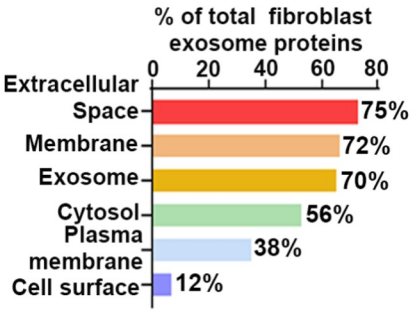

I. Common and unique exosome membrane proteins

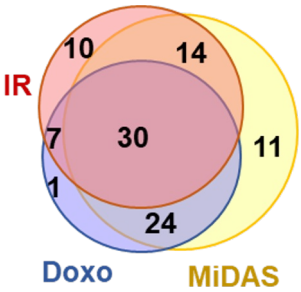

J. Intracellular malondialdehyde (MDA) contents

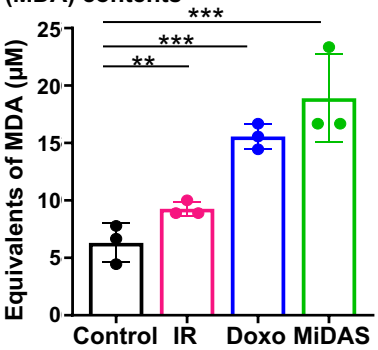

Fig. 3

A. Supervised clustering classifies aging plasma exosomes

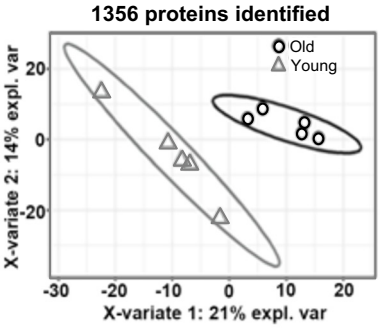

B. Volcano plot showing altered aging plasma exosome proteins

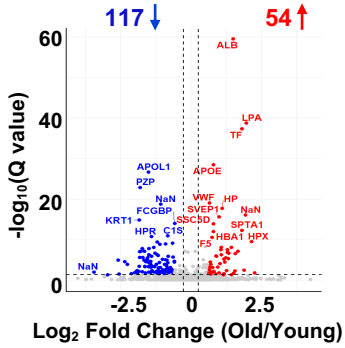

C. Heat map shows differential protein profiles in aging plasma exosome

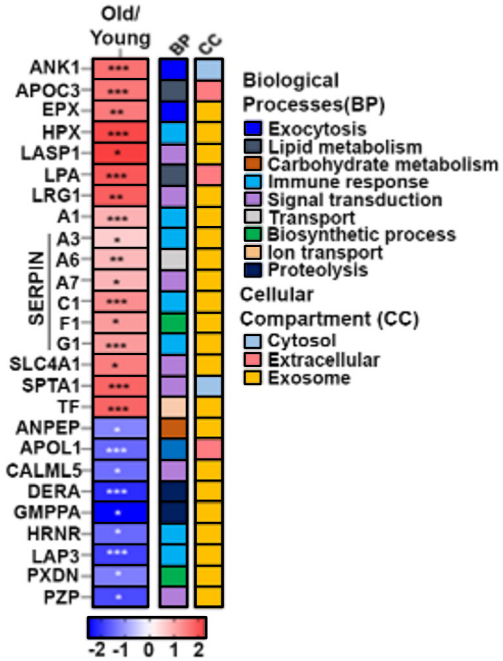

D. Aging plasma exosome protein pathways

(i) Up-regulated

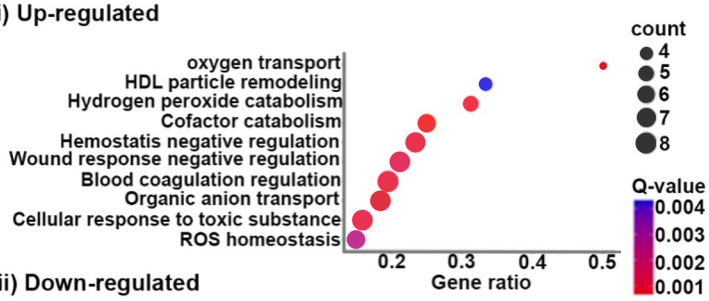

(ii) Down-regulated

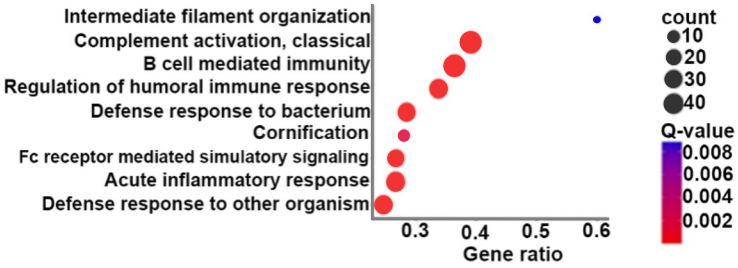

E. *In silico* prediction of plasma exosome cell compartments

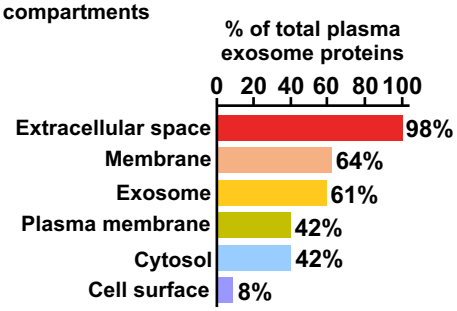

F. Individual protein profiles of plasma exosomes differentially secreted in aging

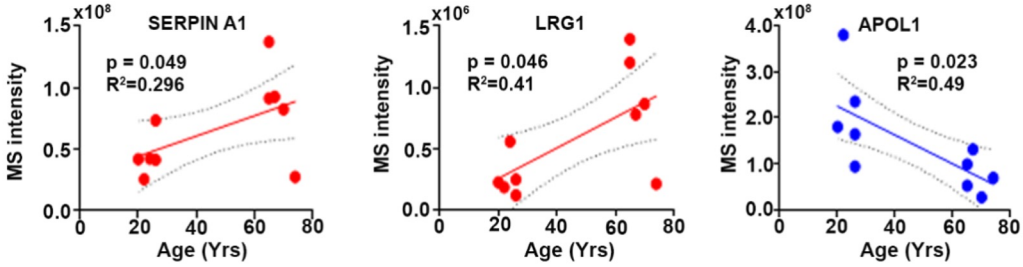

Fig. 4

A. Differential Expression Analysis

Biofluid/ Tissue	# of significant lipids	# of altered lipids	
IR extrinsic	122	115 ↑	7 ↓
Doxo extrinsic	135	123 ↑	24 ↓
MiDAS intrinsic	129	128 ↑	1 ↓

B. Supervised clustering

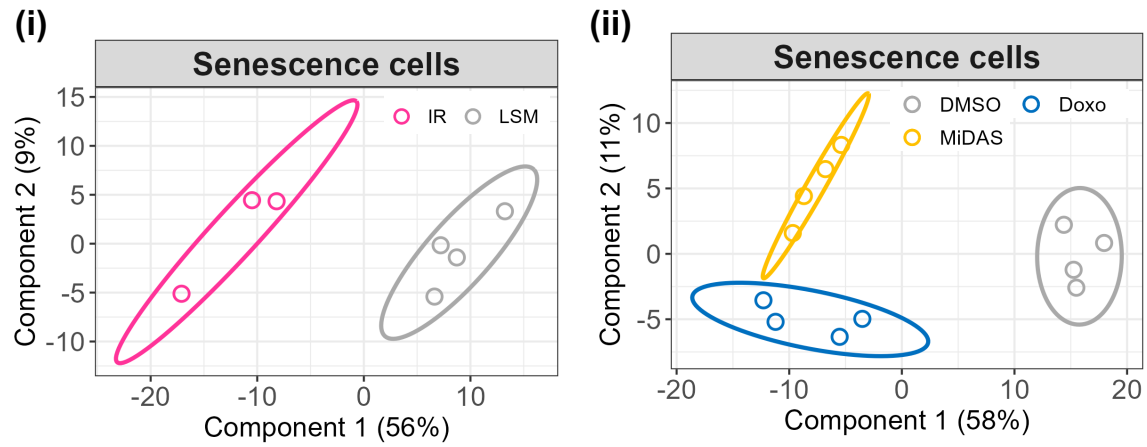

C. Heatmap of differentially expressed lipids

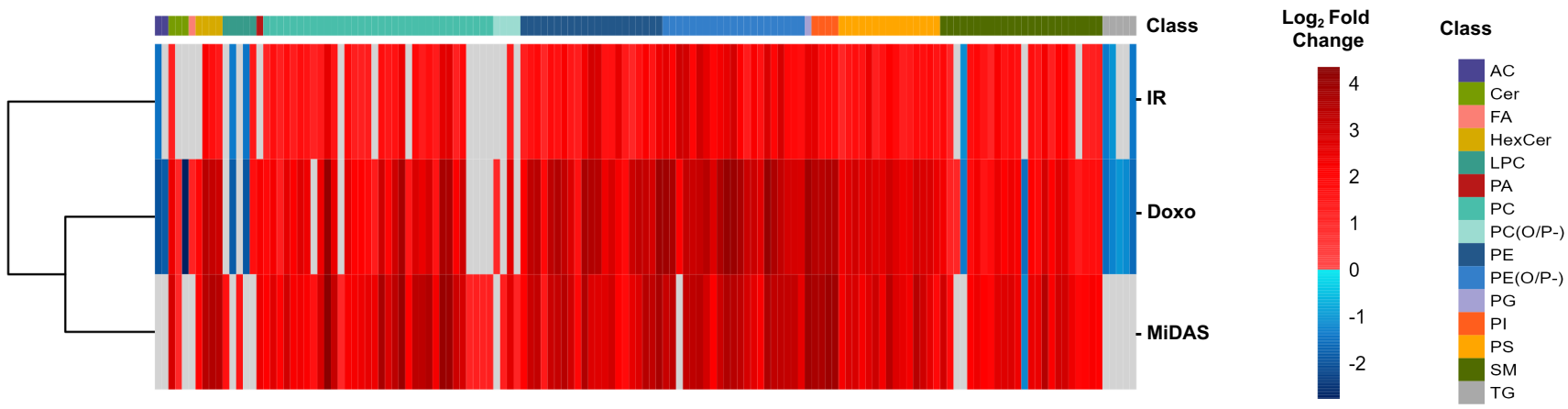

D. Violin plots of selected differentially expressed lipids

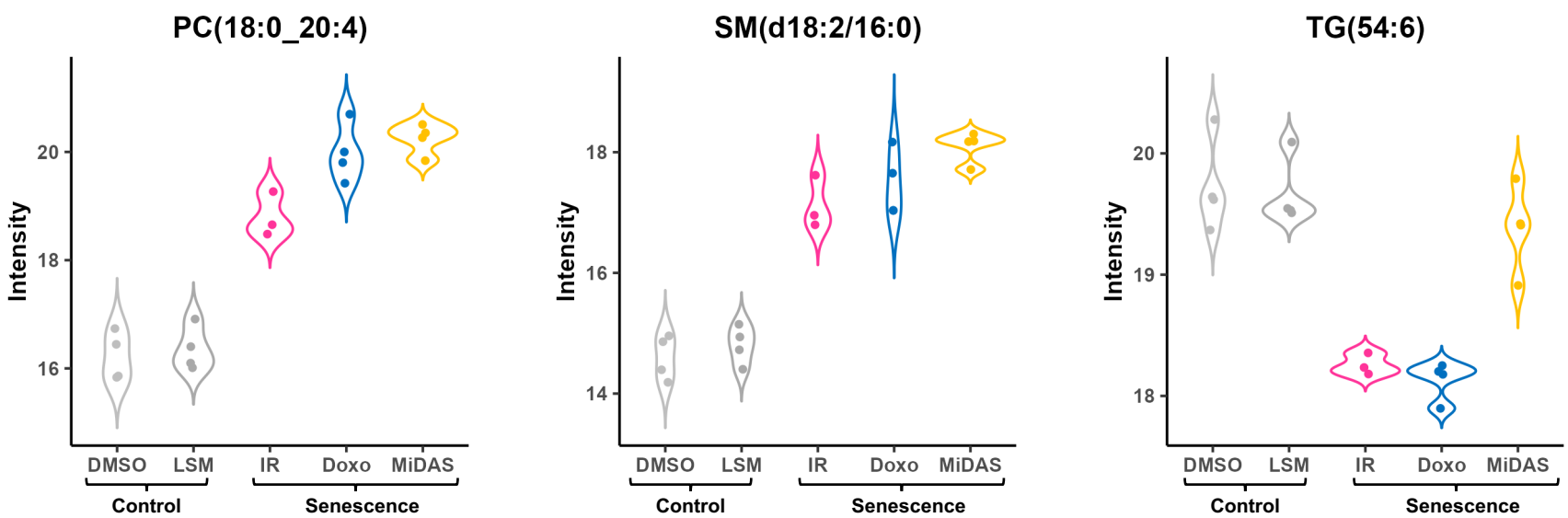

Fig. 5

A. Potential Exosome Biomarkers for Senescence and aging

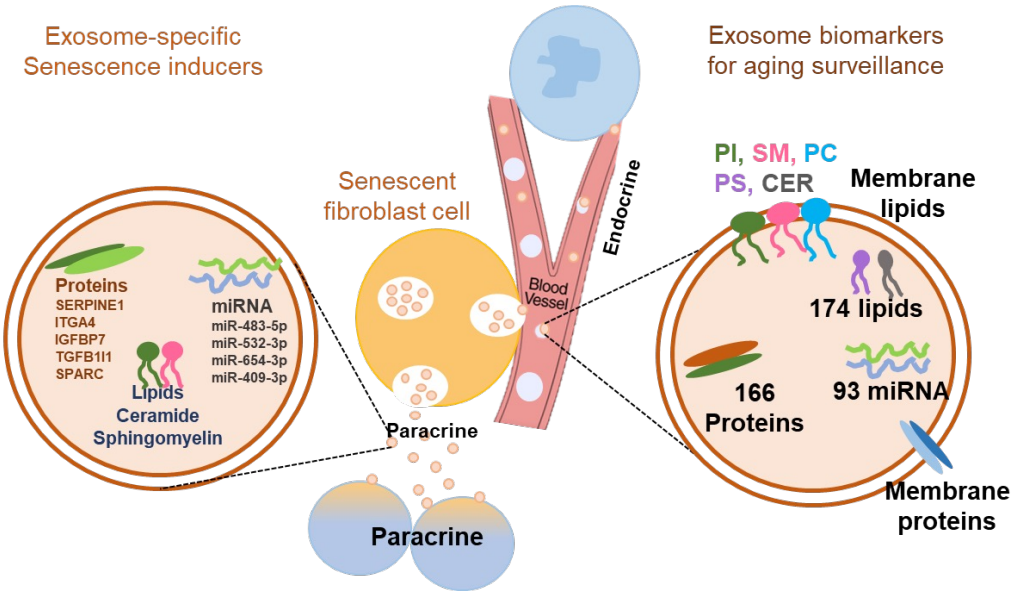

B. Exosome proteins of aged plasma and senescence fibroblasts

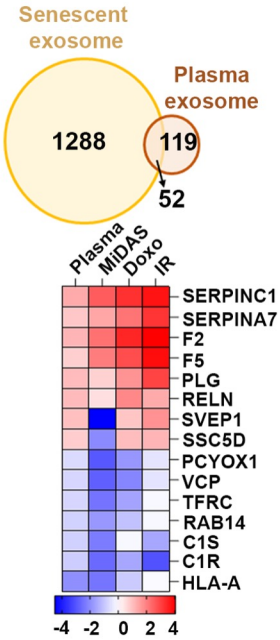

Fig. 6

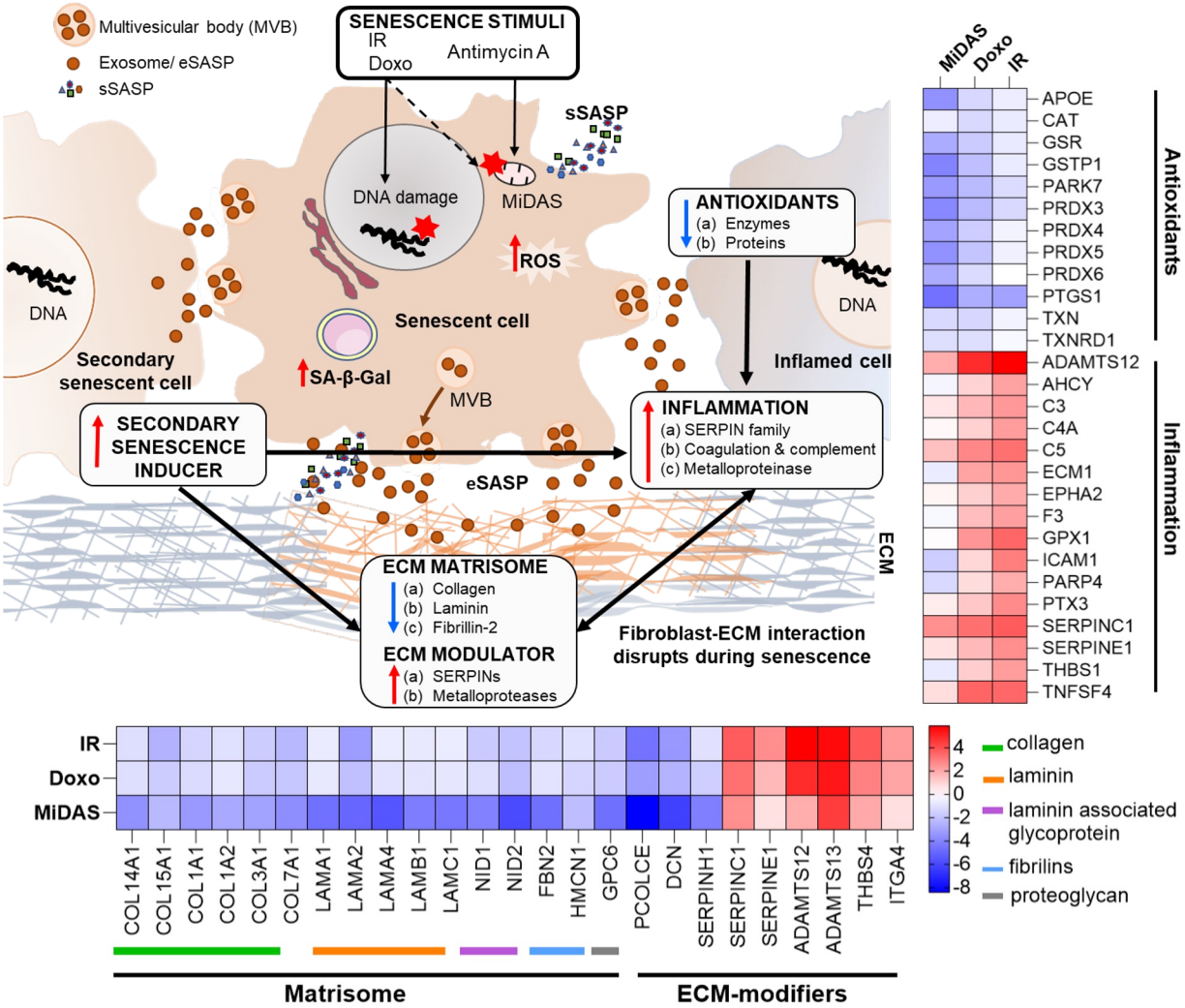
Multivesicular body (MVB)
Exosome/ eSASP
sSASP
SENESCENCE STIMULI
IR
Doxo
Antimycin A
sSASP
DNA damage
MiDAS
ROS
Senescent cell
SA-β-Gal
MVB
DNA
Secondary senescent cell
SECONDARY SENESCENCE INDUCER
eSASP
ANTIOXIDANTS
(a) Enzymes
(b) Proteins
DNA
Inflamed cell
INFLAMMATION
(a) SERPIN family
(b) Coagulation & complement
(c) Metalloproteinase
ECM
ECM MATRISOME
(a) Collagen
(b) Laminin
(c) Fibrillin-2
ECM MODULATOR
(a) SERPINs
(b) Metalloproteases
Fibroblast-ECM interaction disrupts during senescence
MiDAS
Doxo
IR
APOE
CAT
GSR
GSTP1
PARK7
PRDX3
PRDX4
PRDX5
PRDX6
PTGS1
TXN
TXNRD1
ADAMTS12
AHCY
C3
C4A
C5
ECM1
EPHA2
F3
GPX1
ICAM1
PARP4
PTX3
SERPINC1
SERPINE1
THBS1
TNFSF4
Antioxidants
Inflammation
IR
Doxo
MiDAS
COL14A1
COL15A1
COL1A1
COL1A2
COL3A1
COL7A1
LAMA1
LAMA2
LAMA4
LAMB1
LAMC1
NID1
NID2
FBN2
HMCN1
GPC6
PCOLCE
DCN
SERPINH1
SERPINC1
SERPINE1
ADAMTS12
ADAMTS13
THBS4
ITGA4
4
2
0
-2
-4
-6
-8
collagen
laminin
laminin associated glycoprotein
fibrilins
proteoglycan
Matrisome
ECM-modifiers

Fig. 7